Electronic Supplementary Material (ESI) for Polymer Chemistry.
This journal is © The Royal Society of Chemistry 2020

Supporting Information

For

"Impacts of Performing Electrolysis During Organocatalyzed Atom Transfer Radical Polymerization"

Daniel A. Corbin[a], Blaine G. McCarthy[a], Garret M. Miyake[a,*]

[a] Department of Chemistry, Colorado State University, Fort Collins, Colorado 80523-1872, United States of America

* Corresponding author, E-mail: garret.miyake@colostate.edu

Table of Contents

Materials and Methods

Purchased Chemicals

For the Synthesis of Photocatalysts

Phenazine Reduction. Phenazine and sodium hydrosulfite were purchased from Alfa Aesar. Reagent grade alcohol was purchased from Fisher.

Buchwald Couplings. 4-Bromobenzotrifluoride, bis(dibenzylideneacetone)palladium(0), the 1 M tri-*tert*-butylphosphine solution in toluene, and sodium *tert*-butoxide were purchased from Sigma Aldrich. 1-Bromonaphthalene was purchased from VWR. Toluene was purified using an mBraun MB-SPS-800 solvent purification system and kept under nitrogen atmosphere.

Bromination using Molecular Bromine. Bromine was purchased from Beantown Chemical, while benzene was purchased from Sigma Aldrich. Copper wire was purchased from Fisher.

Bromination using *N*-bromosuccinimide. *N*-Bromosuccinimide was purchased from VWR. Unstabilized tetrahydrofuran (THF) was purchased from Millipore Sigma.

Suzuki Coupling. Potassium carbonate, 2-naphthylboronic acid, and tetrakis(triphenylphosphine)palladium(0) were purchased form Sigma Aldrich. 4-Biphenylboronic acid was purchased from TCI America. Unstabilized THF was purchased from Millipore Sigma.

For Polymerizations

N,*N*-Dimethylacetamide (DMAc), methyl methacrylate (MMA), and diethyl-2-bromo-2-methylmalonate (DBMM) were purchased form Sigma Aldrich.

For Electrochemical Experiments

Tetra-n-butylammonium hexafluorophosphate (Bu_4NPF_6), tetra-n-butylammonium bromide (Bu_4NBr), and lithium hexafluorophosphate were purchased from TCI America. Ferrocene, silver nitrate, tetra-n-butylammonium chloride (Bu_4NCl), acetonitrile, and *N*,*N*-dimethylacetamide were purchased from Sigma Aldrich.

Chemical Preparation and Storage

Toluene was purified using an mBraun MB-SPS-800 solvent purification system and kept under nitrogen atmosphere until it was used. MMA and DBMM dried overnight using calcium hydride, vacuum distilled, and degassed by freeze-pump-thaw. They were then stored under nitrogen atmosphere until their use in polymerizations. For electrochemical experiments, MMA was purified to remove inhibitors by passing it through an alumina column. It was then stored in an amber glass bottle in a -25 ºC freezer until its use. Bis(dibenzylideneacetone)palladium(0), tetrakis(triphenylphosphine)palladium(0), DMAc for polymerizations, and lithium hexafluorophosphate were received and stored under inert atmosphere until their use.

Experimental Equipment

Electrodes

All cyclic voltammetry (CV) was performed using a glassy carbon working electrode and a platinum wire counter electrode. Prior to use, the working electrode was polished using a 0.05-micron alumina slurry on a polishing pad, followed by 5 minutes of sonication in DI water and

then 5 minutes of sonication in ethanol. In every case, the reference electrode was either 0.01 M $AgNO_3$/Ag in MeCN with 0.1 M Bu_4NPF_6, or a silver wire quasi-reference electrode (QRE).

For electrolysis, a glassy carbon rod was used as the working electrode and prepared in the same fashion as described above (see working electrode preparation for CV). For the counter electrode, a platinum wire was used. In experiments employing a U-cell, a coiled wire was used to maximize the electrode surface area in contact with the solution. Instead, in experiments employing a 5-neck pear flask (Gamry Dr. Bob's cell), a platinum wire was placed in a Teflon tube with a vycor frit separator on one end and filled with the supporting electrolyte solution. Again, the reference electrode was either 0.01 M $AgNO_3$/Ag in MeCN with 0.1 M Bu_4NPF_6, or a silver wire QRE.

For calibration of the silver wire QRE in 50/50 (*v/v*) DMAc/MMA with 0.1 M Bu_4NPF_6 (94%) and Bu_4NBr (6%), cyclic voltammetry of ferrocene (Fc) was performed to obtain an $E_{1/2}$ (Fc/Fc^+) = 0.903 V.

Electrolysis Cells

For work employing a U-cell for electrolysis, a custom cell was designed and built by scientific glassblower Michael Olsen at Colorado State University. The cell features a working and counter electrode compartment, separated by an extra-fine glass frit (Figure S1). Both compartments were fitted with ground glass joints, allowing for further customization as needed, and the working compartment was designed to include a side-arm for the reference electrode to be inserted to the solution.

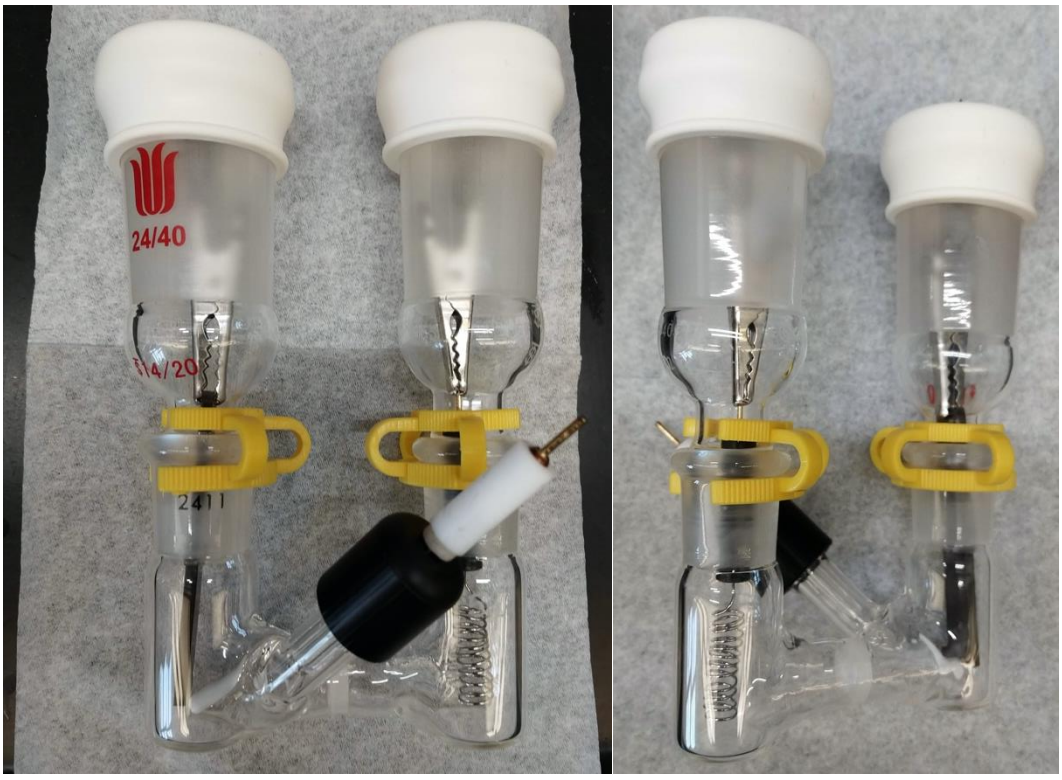

Figure S1. Photographs of the U-cell used in this work. (Left) Front side of the cell, showing the working electrode compartment on the left side, with a glassy carbon working electrode and reference electrode inserted in the side-arm. In the center, an extra-fine glass frit acts as a separator

to prevent reaction solution from contacting the counter electrode, which is displayed in the right-side compartment. (Right) View of the U-cell from the back-side.

For work employing a 5-neck pear flask, a Gamry Dr. Bob's cell was used (part number: 990-00193). To achieve separation of the counter electrode in this cell, a teflon tube was fitted with a vycor glass frit (Gamry Porous Glass Frit, part number: 955-00003) and inserted into the cell. In addition, the working and counter electrodes were inserted through separate ports, and a ground glass nitrogen adapter was used to maintain the cell under inert atmosphere (Figure S2).

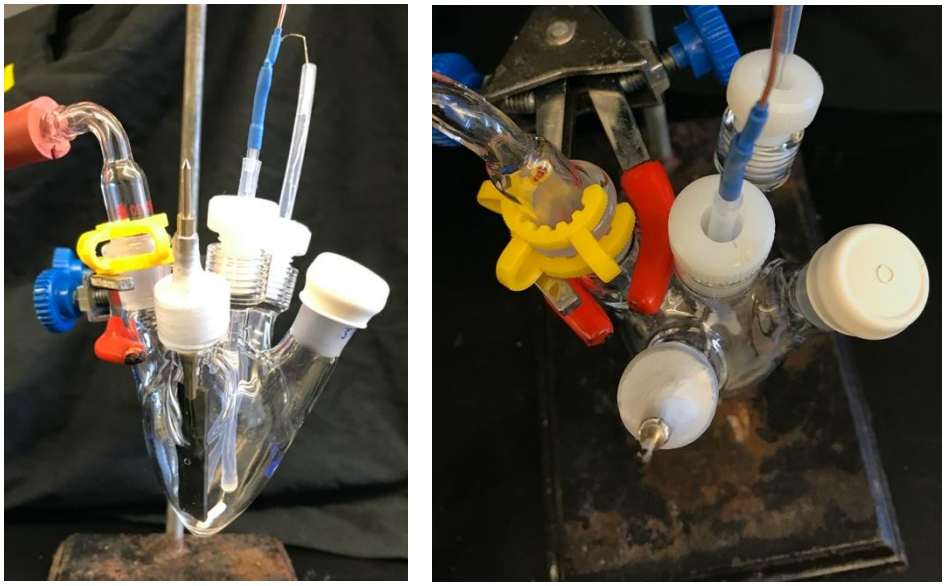

Figure S2. Photographs of the 5-neck electrochemical cell used in this work. (Left) A side view of the cell, showing (from left to right) the nitrogen gas inlet, working electrode, reference electrode, counter electrode (with separator), and sampling port. (Right) A top-down view of the cell showing the various ports.

Light Reactors

The following LEDs were used in the construction of light reactors for this work. For light beakers, strips of water-resistant white LEDs were purchased from Creative Lighting Solutions (item no. CL-FRS5050WPDD-5M-12V-WH). For LED wells, strips of white LEDs were purchased from Creative Lighting Solutions (item no. CL-FRS1210-5M-12V-WH). For high-power light reactors, cool white LED emitters were purchased from LED Engin (item no. LZ4-00CW08). For LED dimming, a Dragonpad 12V12A inline mini LED dimmer control for single color LED strip lights with 7 dimmer settings was installed between the power supply and LED strip. Correlation between dimmer settings and percent LED intensity was obtained from previously published measurements.[1]

Below, the various light reactors used in this work are pictures and described:

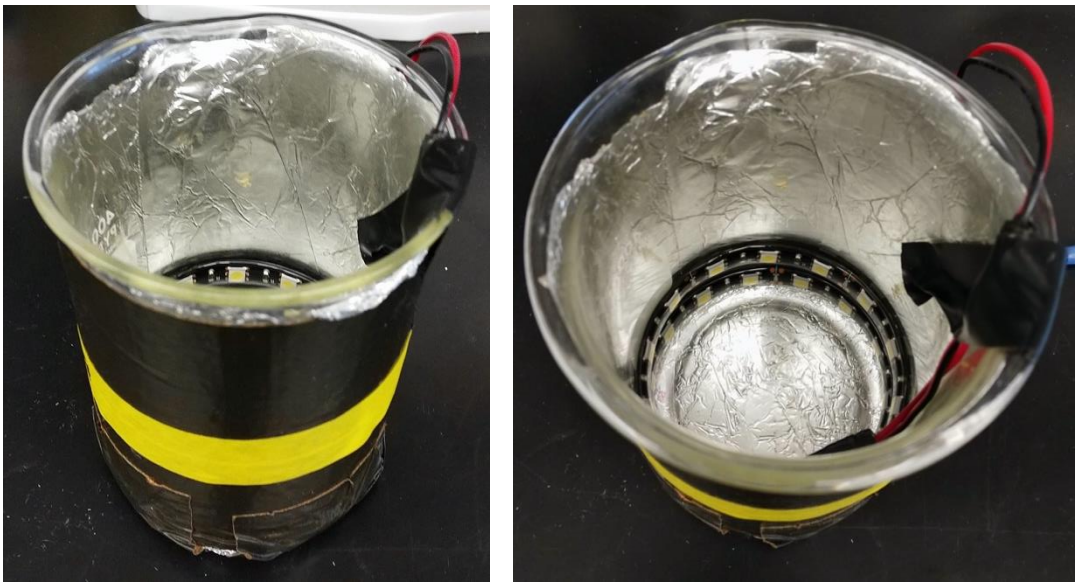

Figure S3. Photographs of the LED beaker used in this work from the front (left) and top (right). The reactor was constructed by wrapping a 400 mL beaker (10.0 cm tall, 8.5 cm diameter) with aluminum foil and wrapping a coated white LED strip (9 LED segments, 16” total) inside the bottom of the beaker.

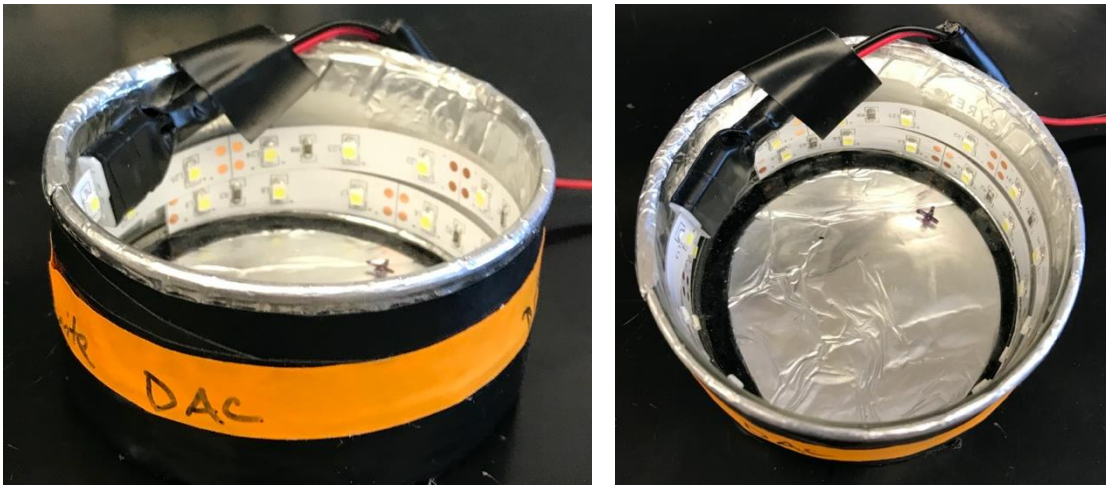

Figure S4. Photographs of the LED wells used in the majority of this work. These reactors were built by wrapping an 80 mm x 40 mm recrystallization dish with aluminum foil and wrapping uncoated white LED strips (9 LED segments) around the inside of the disk. The photographs provide a side view (left) and top view (right).

Figure S5. Photographs of the LED wells constructed with more light strips. These reactors were built by wrapping an 80 mm x 40 mm recrystallization dish with aluminum foil and wrapping uncoated white LED strips (15 LED segments) around the inside of the disk. The photographs provide a side view (left) and top view (right).

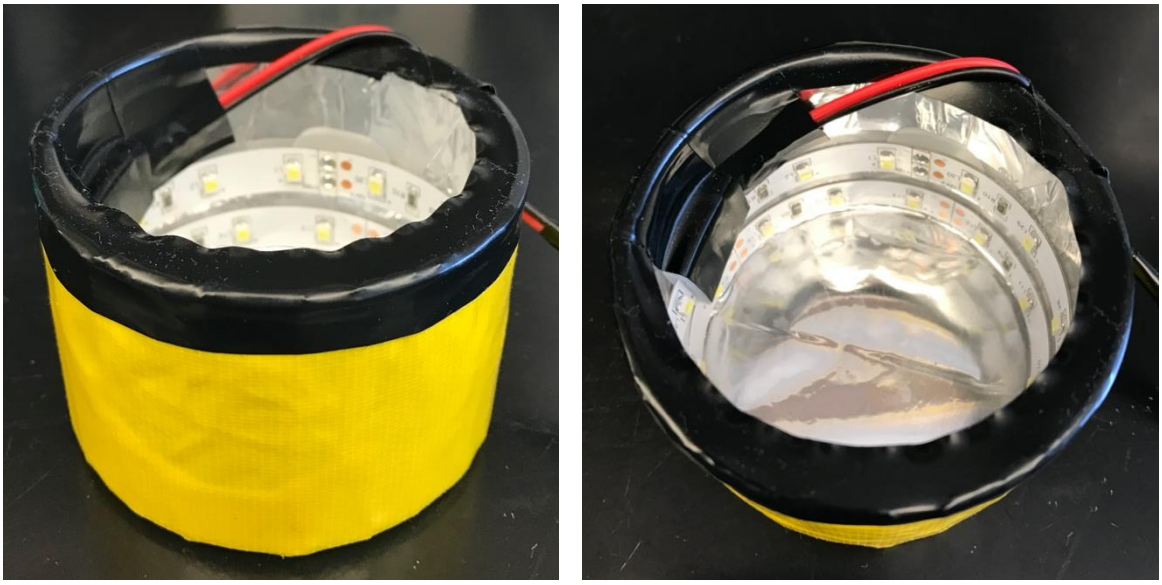

Figure S6. Photographs of the LED wells constructed to move the LEDs closer to the reaction vessel. These reactors were built by wrapping a 70 mm x 50 mm recrystallization dish with aluminum foil and wrapping uncoated white LED strips (9 LED segments) around the inside of the disk. The photographs provide a side view (left) and top view (right).

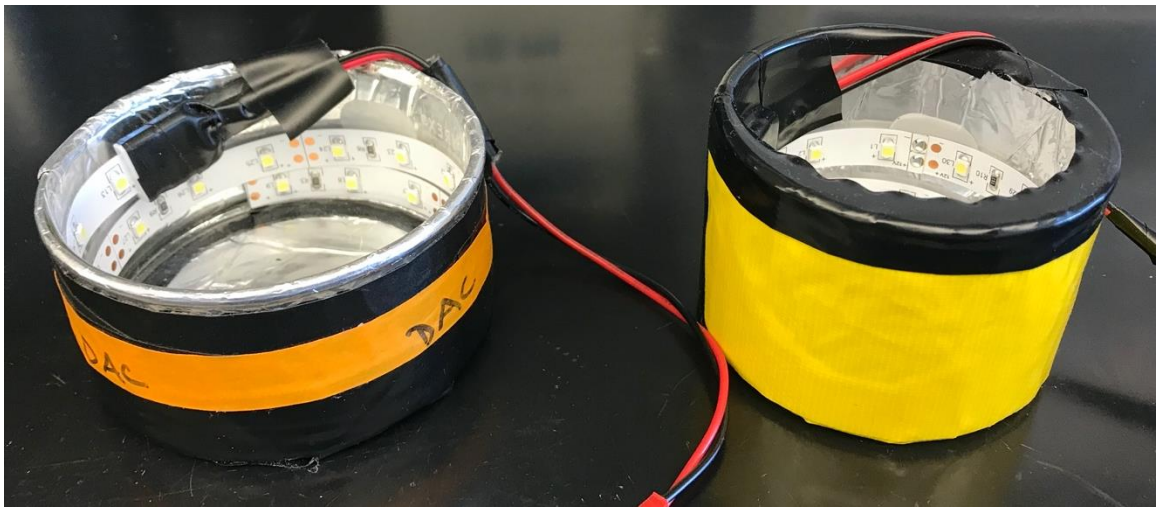

Figure S7. Photograph comparing the original light well used in this work (left, dimensions: 80 x 40 with 9 LED segments) and that constructed to move the LEDs closer to the reaction vessel (right, dimensions: 70 x 50 with 9 LED segments).

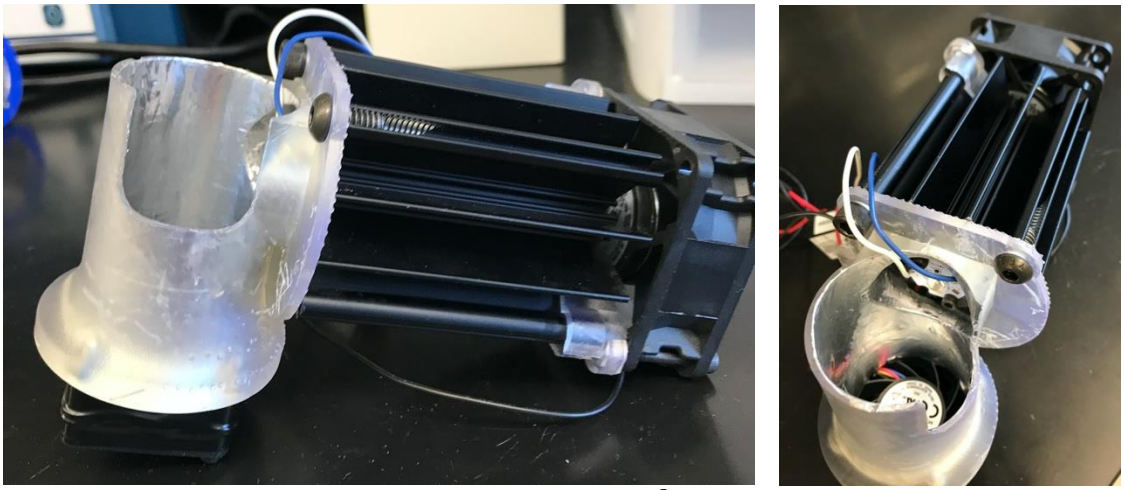

Figure S8. Photographs of the high-power LED reactor[2] designed for use with the U-cell. (Left) A side view of the reactor, showing the 3D-printed reactor body, which can be designed and exchanged depending on the flask being used. Attached to this reactor body is a cooling fan (bottom) used to maintain the temperature of the reaction vessel, as well as a cooling fin connected to the LED and another cooling fan used to regulate the temperature of the LED. (Right) Top view of the reactor body, showing the LED attached to the cooling fin and the LED that points inside of the reactor body.

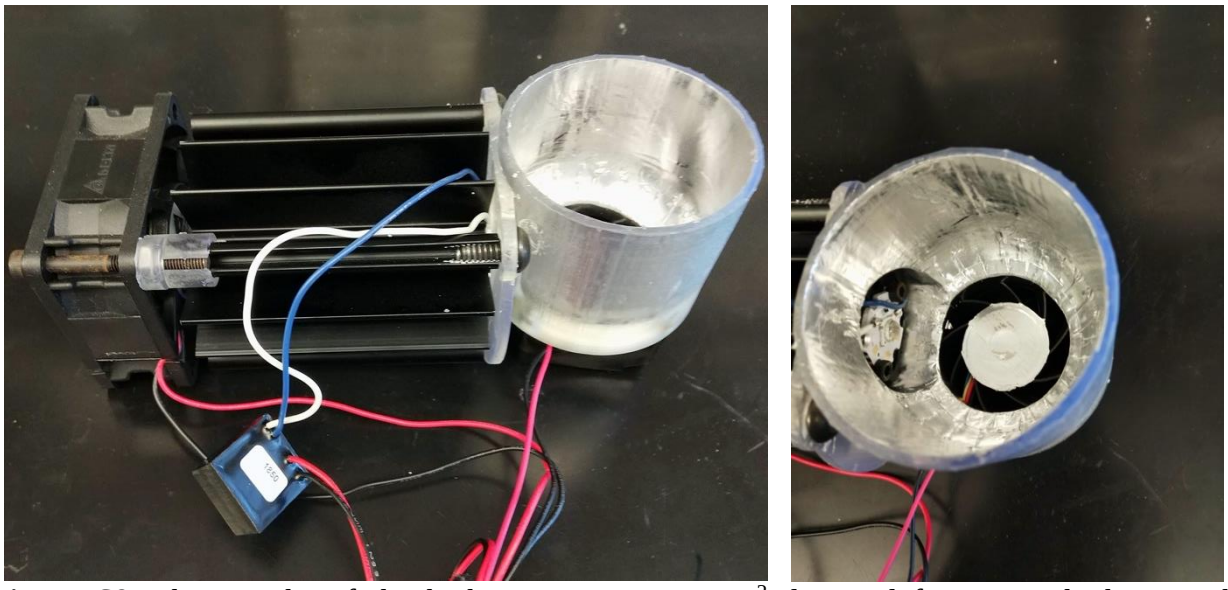

Figure S9. Photographs of the high-power LED reactor[2] designed for use with the 5-neck electrochemical cell. (Left) A side view of the reactor, showing a cooling fan (left) connected to cooling fins (center) that maintain the temperature of the LED. On the right side of the cooling fin is a 3D-printed reactor body, which can be designed and exchanged depending on the flask being used. (Right) Top view of the reactor body, showing the LED attached to the cooling fin and another cooling fan on the bottom of the reactor body used to control the temperature of the reaction vessel.

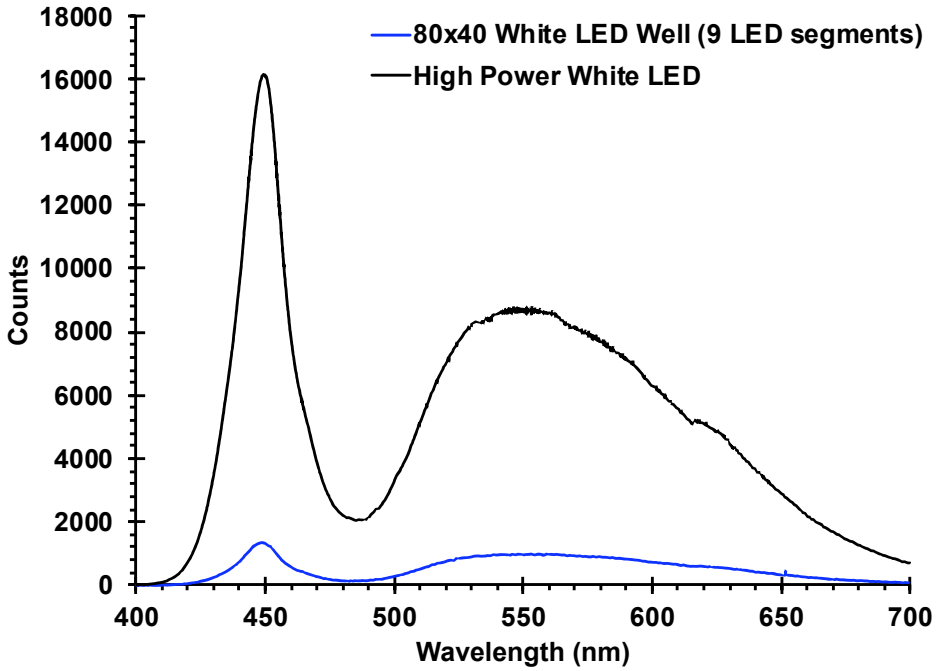

FigureSAV-10. Qualitative emission spectra of white LEDs used in this work: white LEDs used in light wells (blue) and high-power light reactors (black).

Instrumentation

Nuclear magnetic resonance (NMR) spectroscopy was performed using either a Bruker US 400 MHZ spectrometer or a Bruker Ascend 400 MHZ spectrometer. All ^{1}H NMR spectra are reported in **δ** units, parts per million (ppm), and are referenced to residual chloroform (7.26 ppm) or benzene (7.15) signals. Analysis of polymer molecular weights were performed via gel permeation chromatography (GPC) coupled with multi-angle light scattering (MALS), using an Agilent HPLC fitted with one guard column, three PLgel 5 μm MIXED-C gel permeation columns, a Wyatt Technology TrEX differential refractometer, and a Wyatt Technology miniDAWN TREOS light scattering detector, using THF as the eluent at a flow rate of 1.0 mL/min and a dn/dc value of 0.084. Electrochemical measurements were performed using either a Gamry Interface 1010B or 1010E potentiostat. UV-Visible spectroscopy was performed using an Agilent Cary 5000 UV-Vis-NIR spectrometer. Measurements of LED emission were made using an Olympus IX73 inverted microscope connected to a Horiba iHR 550 spectrometer with a Horiba Synapse back-illuminated CCD camera and a 1200 blaze/mm grating. For qualitative measurements of LED emission intensity, light sources were placed in the same configuration and the light directed into an opening in the microscope.

Procedures

Photocatalyst Synthesis

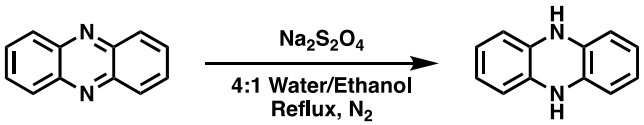

Figure S11. Scheme for the synthesis of 5,10-dihydrophenazine by reduction of phenazine.

Synthesis of 5,10-dihydrophenazine. Dihydrophenazine used in this work was synthesized using a published literature procedure.[3]

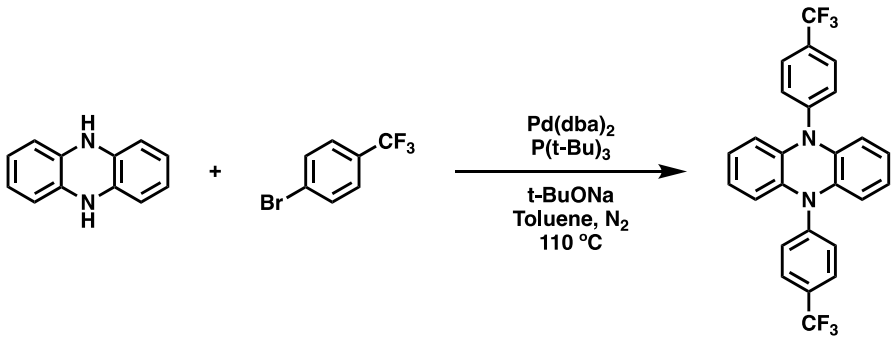

Figure S12. Scheme for the synthesis of 5,10-di(4-trifluorobenzo)-5,10-dihydrophenazine *via* Buchwald coupling.

Synthesis of 5,10-di(4-trifluorobenzo)-5,10-dihydrophenazine. A modified literature procedure as used.[4] A Schlenk flask was charged with sodium *tert*-butoxide (3.173 g, 33.02 mmol, 3 eq) and degassed. Using standard Schlenk techniques, 4-bromobenzotrifluoride (3.84 mL, 27.5 mmol, 2.5 eq), which had been degassed by nitrogen bubbling, was added to the flask. The reaction flask was then brought into a nitrogen filled glovebox, where dihydrophenazine (1.9997 g, 10.974 mmol, 1 eq), bis(dibenzylideneacetone)palladium(0) (130.4 mg, 0.2268 mmol, 0.02 eq), tri-*tert*-butylphosphine (1 M solution in toluene, 0.68 mL, 0.66 mmol, 0.06 eq), and toluene (40 mL) were added to the flask. The reaction was then refluxed at 110 ºC for 44 h, after which it was cooled to room temperature. The reaction mixture was then combined with dichloromethane (DCM, 200 mL), causing a yellow precipitate to form. The solid was collected by vacuum filtration and washed with cold DCM. Further purification was achieved by sublimation (190 ºC, 50 mtorr) to yield 3.4470 g of product (66.7%). NMR characterization (^{1}H and ^{19}F in C_6D_6) matched previously published data.[3]

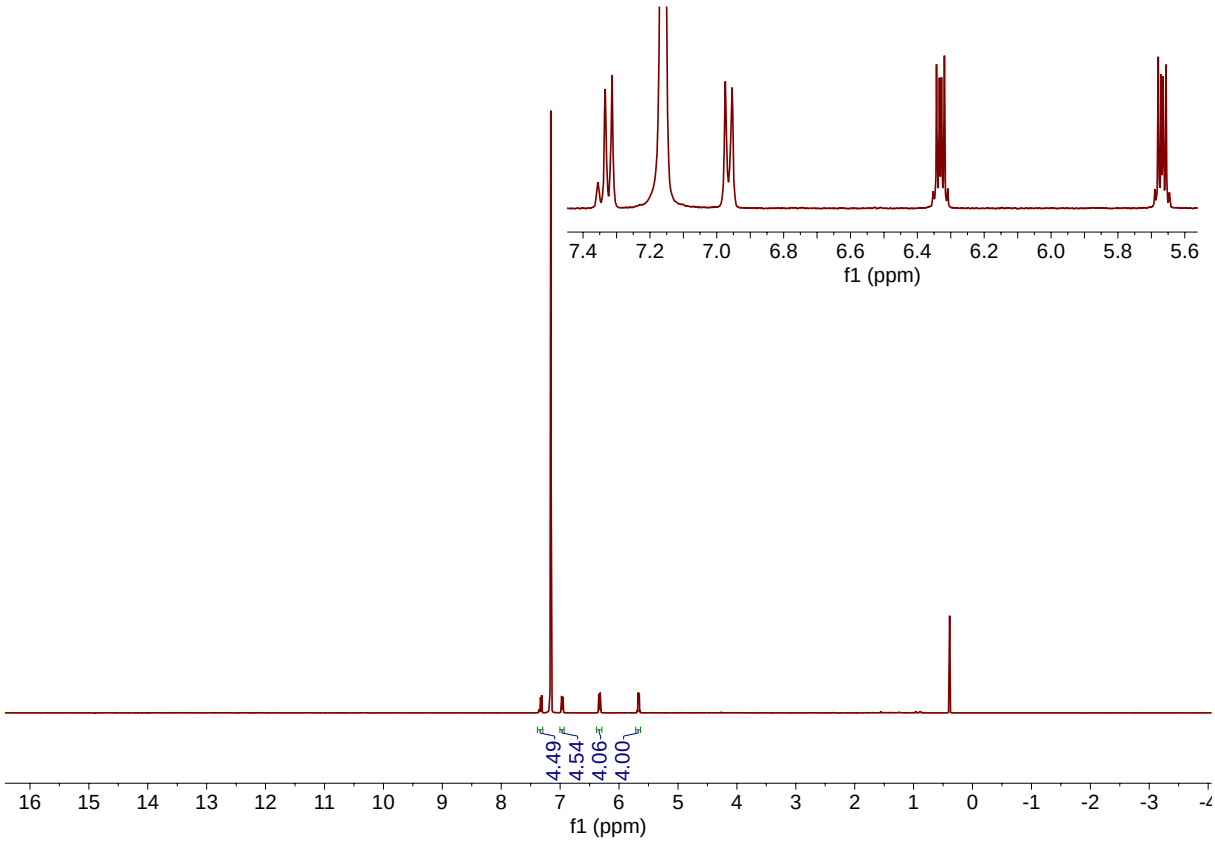

Figure S13. ^{1}H NMR spectrum of 5,10-di(4-trifluorobenzo)-5,10-dihydrophenazine in C_6D_6.

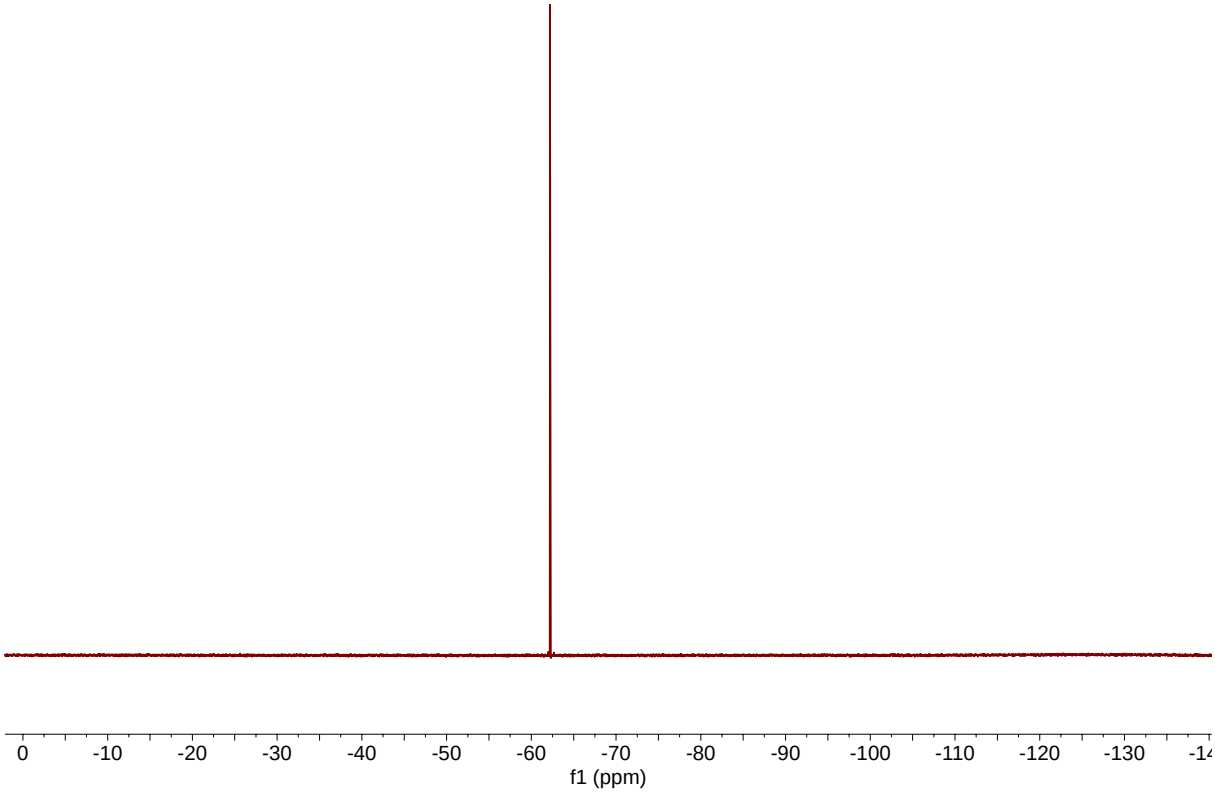

Figure S14. ^{19}F NMR spectrum of 5,10-di(4-trifluorobenzo)-5,10-dihydrophenazine in C_6D_6.

Substitution of the dihydrophenazine core with aryl-functional groups was achieved by following a published literature procedure.[5]

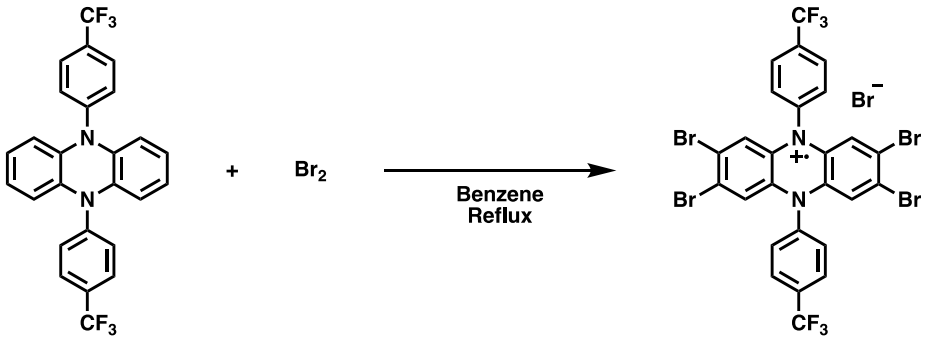

Figure S15. Scheme for the bromination of 5,10-di(4-trifluorobenzo)-5,10-dihydrophenazine using molecular bromine.

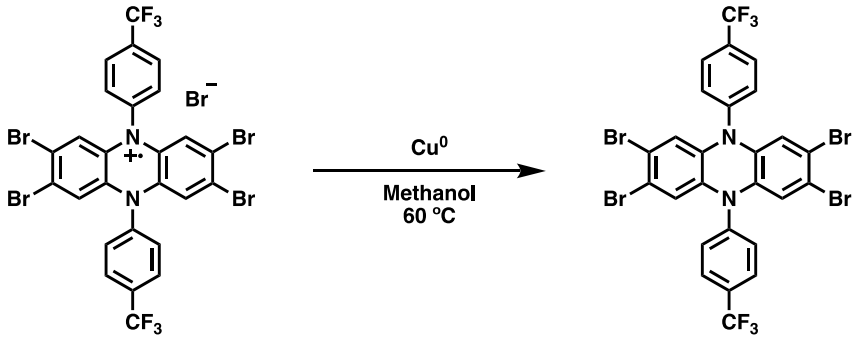

Figure S16. Scheme for the reduction of the radical cation resulting from the bromination of 5,10-di(4-trifluorobenzo)-5,10-dihydrophenazine.

Synthesis of 2,3,7,8-tetrabromo-5,10-di(4-trifluorobenzo)-5,10-dihydrophenazine. Bromination of 5,10-di(4-trifluorobenzo)-5,10-dihydrophenazine and reduction of the subsequent radical cation was carried out according to a published literature procedure.[5]

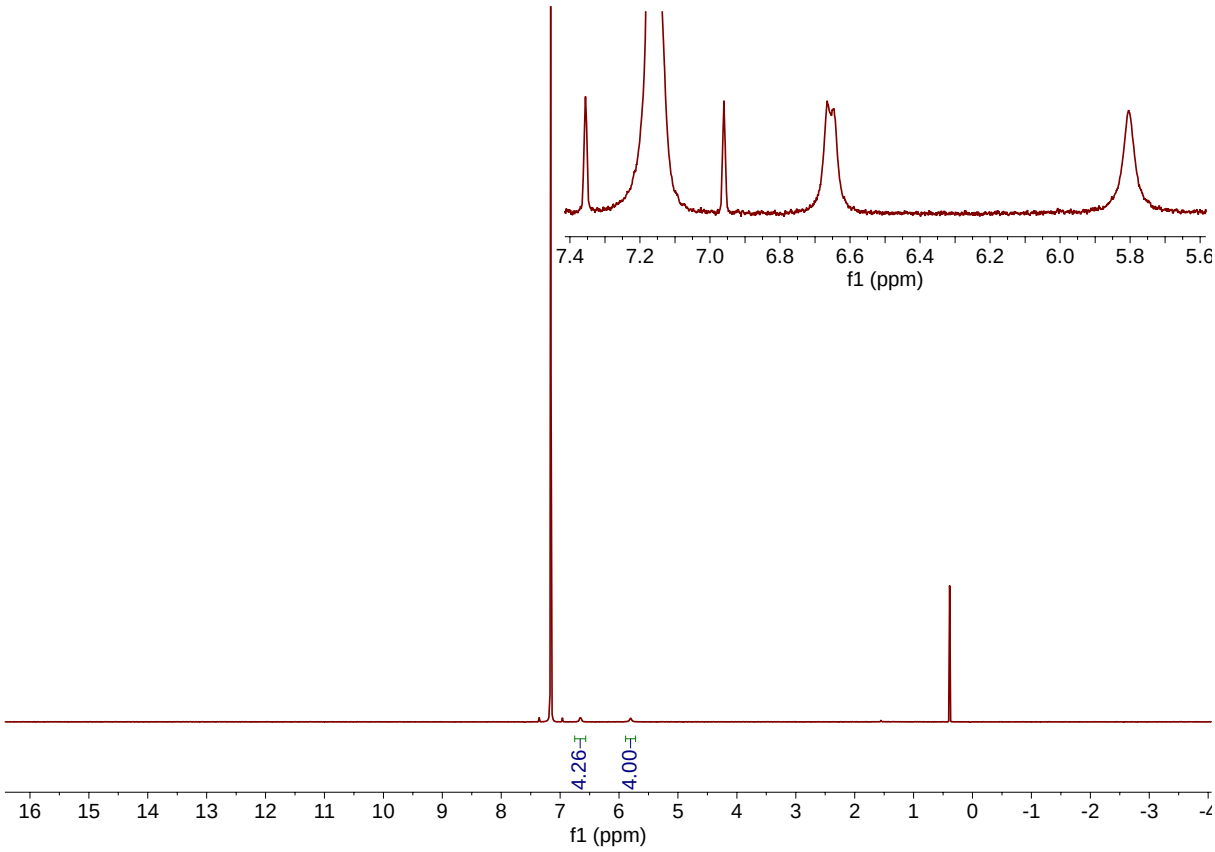

Figure S17. ^{1}H NMR spectrum of 2,3,7,8-tetrabromo-5,10-di(4-trifluorobenzo)-5,10-dihydrophenazine in C_6D_6.

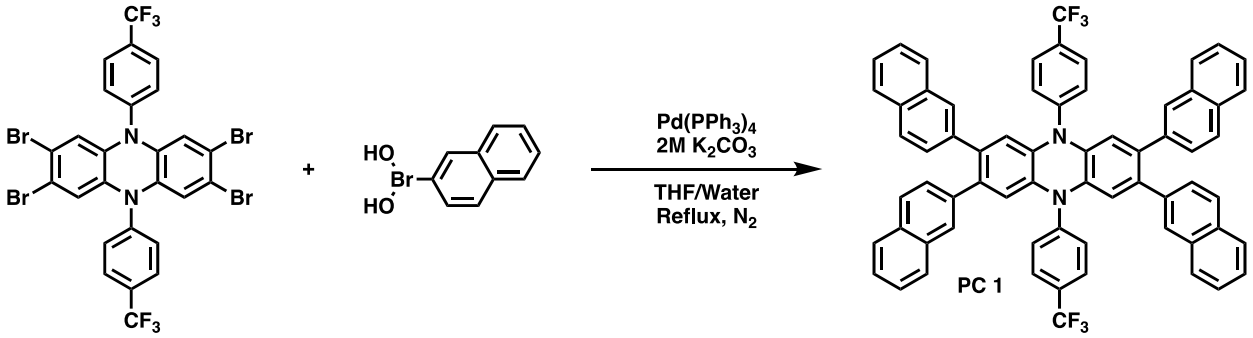

Figure S18. Scheme for the synthesis of 2,3,7,8-tetra(2-naphthyl)-5,10-di(4-trifluorobenzo)-5,10-dihydrophenazine (**1**) *via* Suzuki coupling.

Synthesis of 2,3,7,8-tetra(2-naphthyl)-5,10-di(4-trifluorobenzo)-5,10-dihydrophenazine (1). Synthesis of PC **1** was performed according to a published literature procedure and purified by a modified procedure.[5] A Schlenk flask was charged with 2,3,7,8-tetrabromo-5,10-di(4-trifluorobenzo)-5,10-dihydrophenazine (1.996 g, 2.533 mmol, 1 eq) and 2-naphthylboronic acid (3.504 g, 20.37 mmol, 8 eq). The flask was degassed and brought into a nitrogen filled glovebox, where tetrakis(triphenylphosphine)palladium(0) (299.3 mg, 0.2590 mmol, 0.1 eq) was added to the reaction. The flask was then removed from the glovebox, and THF (200 mL) and potassium carbonate (2M in degassed DI water, 25.4 mL, 50.8 mmol, 20 eq) were added to the reaction. The solution was then heated at 100 ºC for 48 h, after which it was cooled to room temperature and 200 mL DCM was added to the flask. The yellow precipitate that formed was collected by vacuum filtration and further purified by recrystallization from hot DCM and methanol at 0 ºC, yielding 0.8143 g of product (32.9%). NMR characterization (^{1}H in C_6D_6) matched that previously reported for this compound.[5]

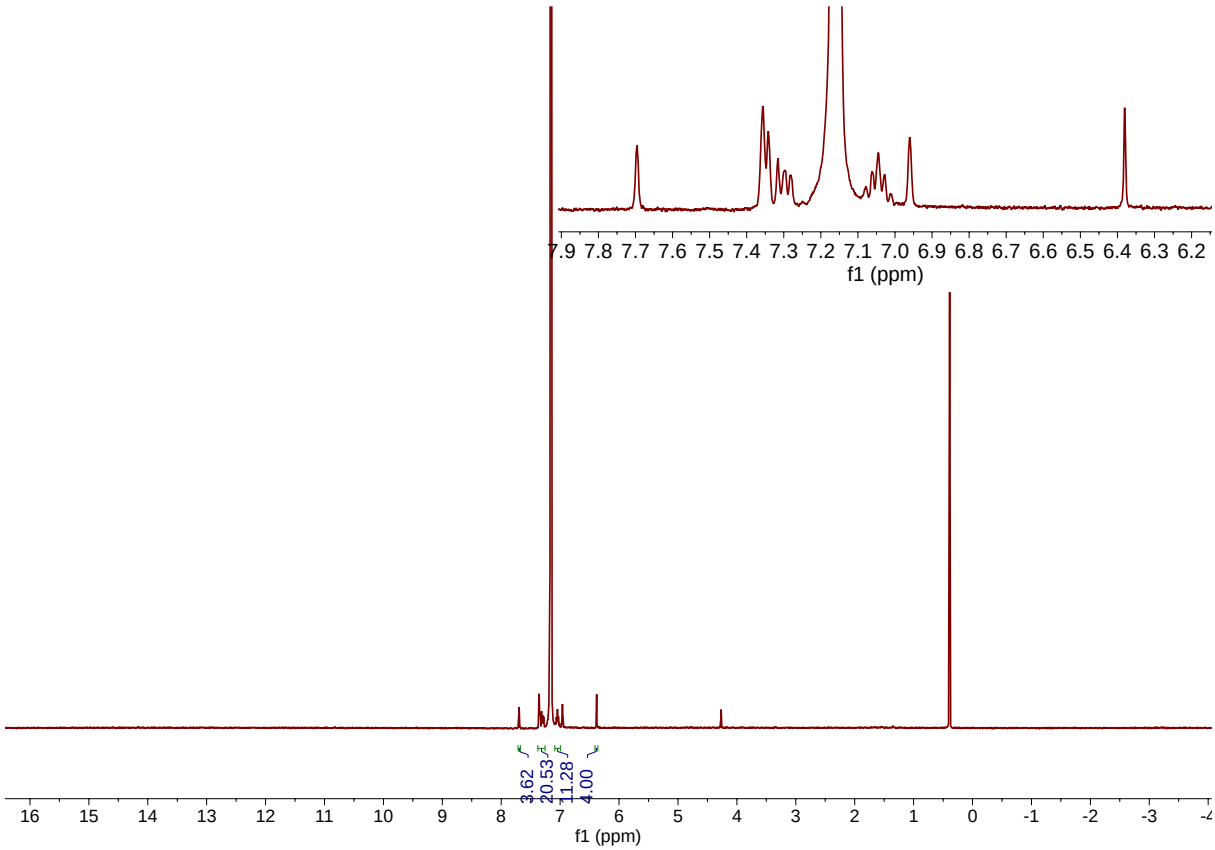

Figure S19. ^{1}H NMR spectrum of **1** in C_6D_6.

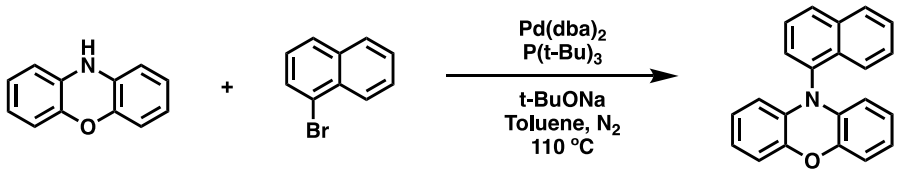

Figure S20. Scheme for the synthesis of 1-naphthyl-10-phenoxazine *via* Buchwald coupling.

Synthesis of 1-naphthyl-10-phenoxazine. Synthesis of 1-naphthyl-10-phenoxazine was performed according to a published literature procedure.[6]

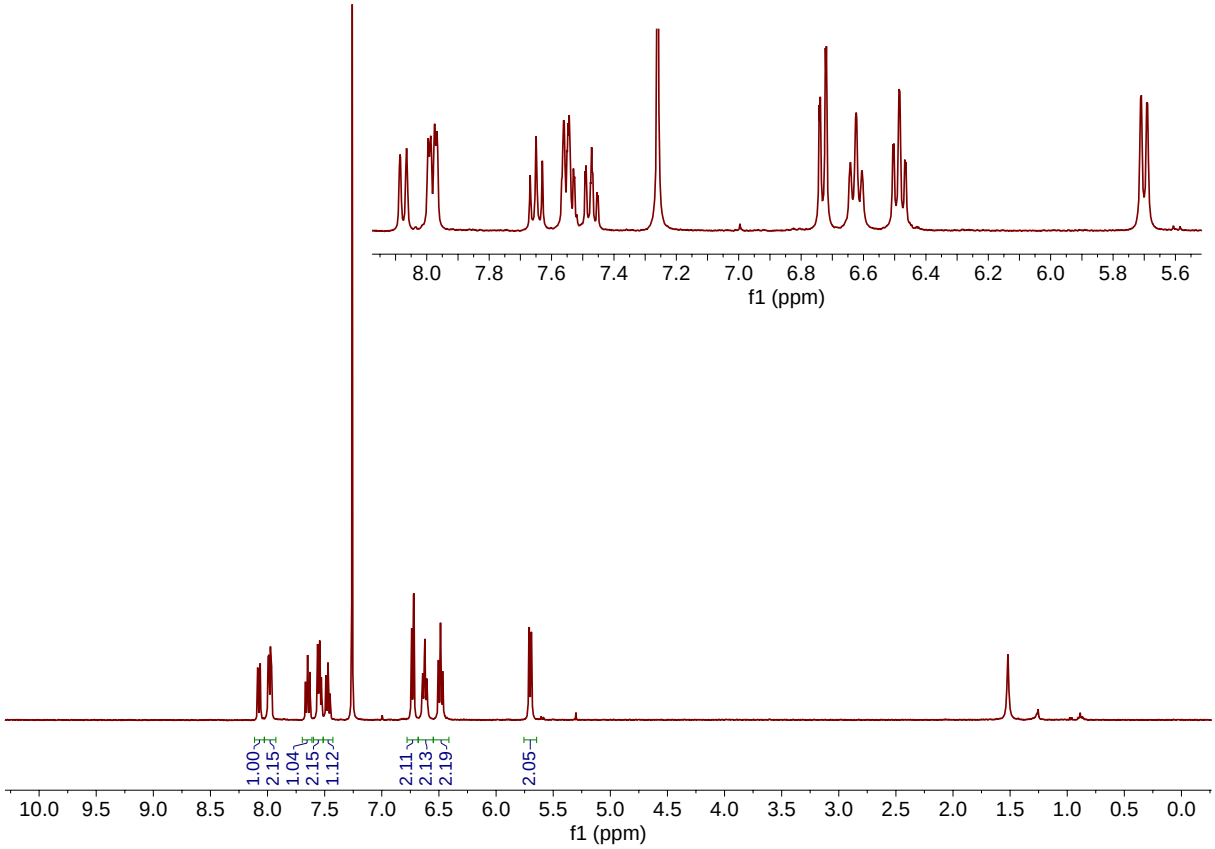

Figure S21. ^{1}H NMR spectrum of 1-naphthyl-10-phenoxazine in $CDCl_3$.

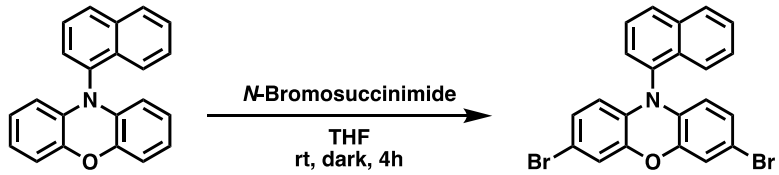

Figure S22. Scheme for the bromination of 1-naphthyl-10-phenoxazine.

Synthesis of 3,7-dibromo-1-naphthyl-10-phenoxazine. Bromination of 1-naphthyl-10-phenoxazine was performed according to a published literature procedure.[6]

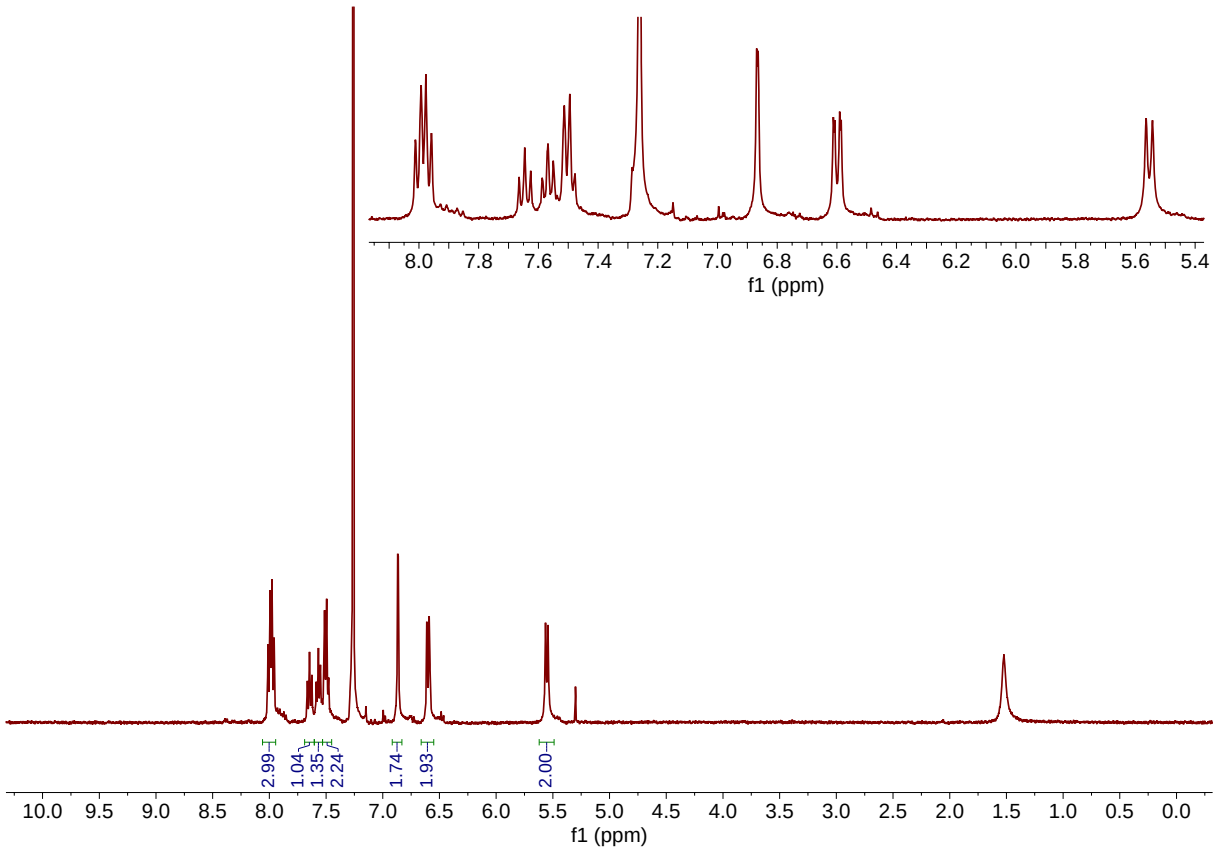

Figure S23. ^{1}H NMR spectrum of 3,7-dibromo-1-naphthyl-10-phenoxazine in $CDCl_3$.

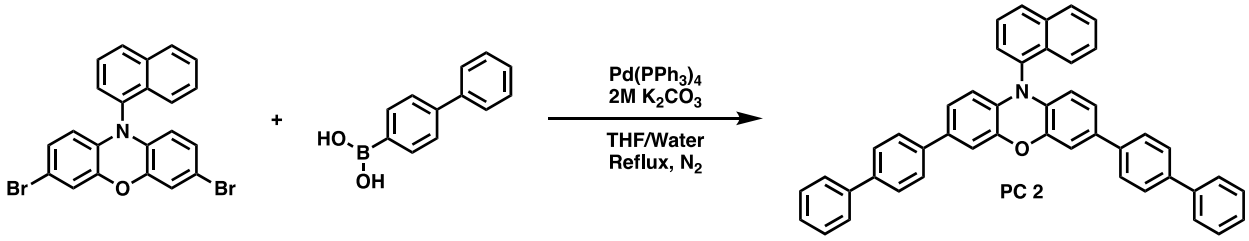

Figure S24. Scheme for the synthesis of 3,7-di(4-biphenyl)-1-naphthyl-10-phenoxazine (**2**) *via* Suzuki coupling.

Synthesis of 3,7-di(4-biphenyl)-1-naphthyl-10-phenoxazine (2). Synthesis of PC **2** was carried out according to a published literature procedure.[6]

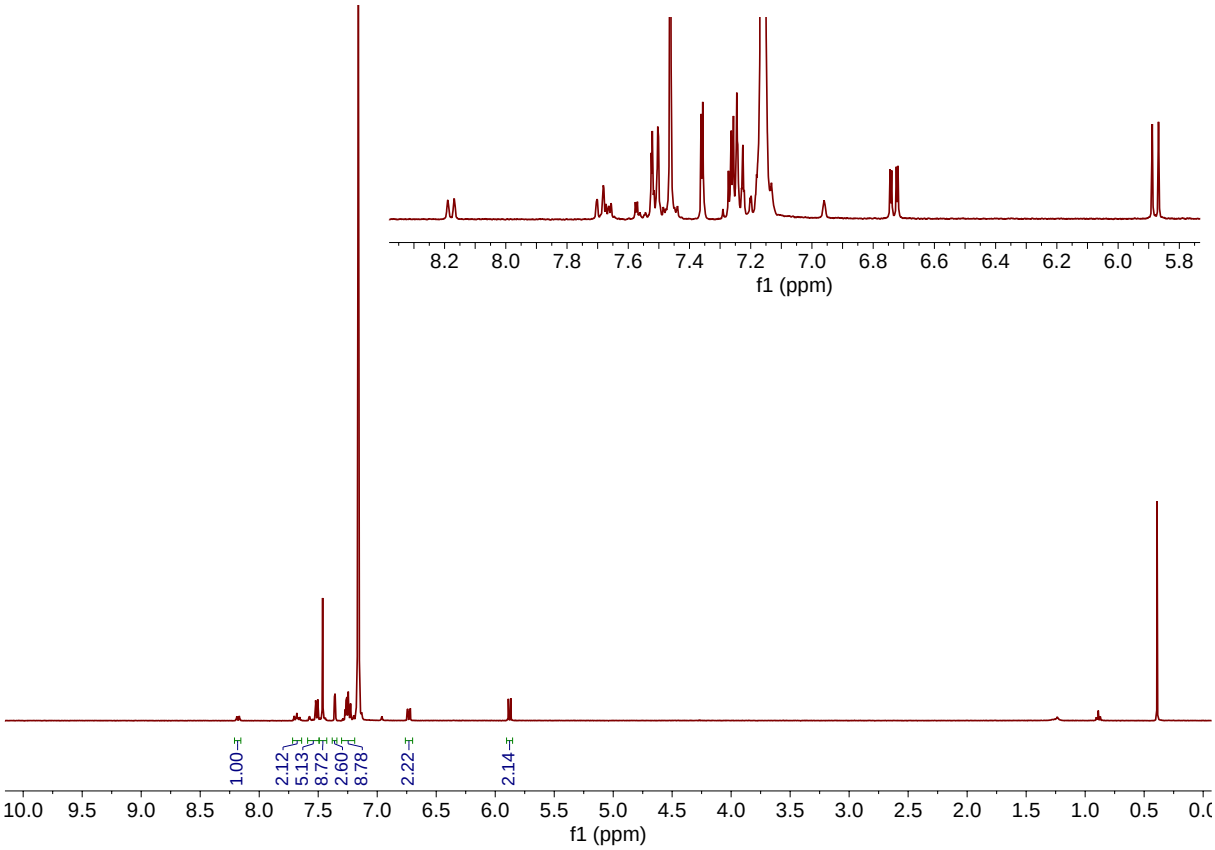

Figure S25. ^{1}H NMR spectrum of 3,7-di(4-biphenyl)-1-naphthyl-10-phenoxazine in C_6D_6.

Cyclic Voltammetry of PCs 1 and 2

To determine the appropriate electrochemical potentials to apply during eO-ATRP, catalysts were characterized by cyclic voltammetry (CV) in 50/50 (*v/v*) DMAc/MMA to mimic polymerization conditions. From the resulting cyclic voltammogram, the $E_{1/2}$ of the PC was determined to approximate the standard reduction potential (E^o). For all measurements reported, the solution was sparged with N_2 for 5 minutes prior to measurement, the working electrode was a glassy carbon disk, and the counter electrode was composed of Pt. Reference electrodes and supporting electrolytes used are stated in the respective figure captions.

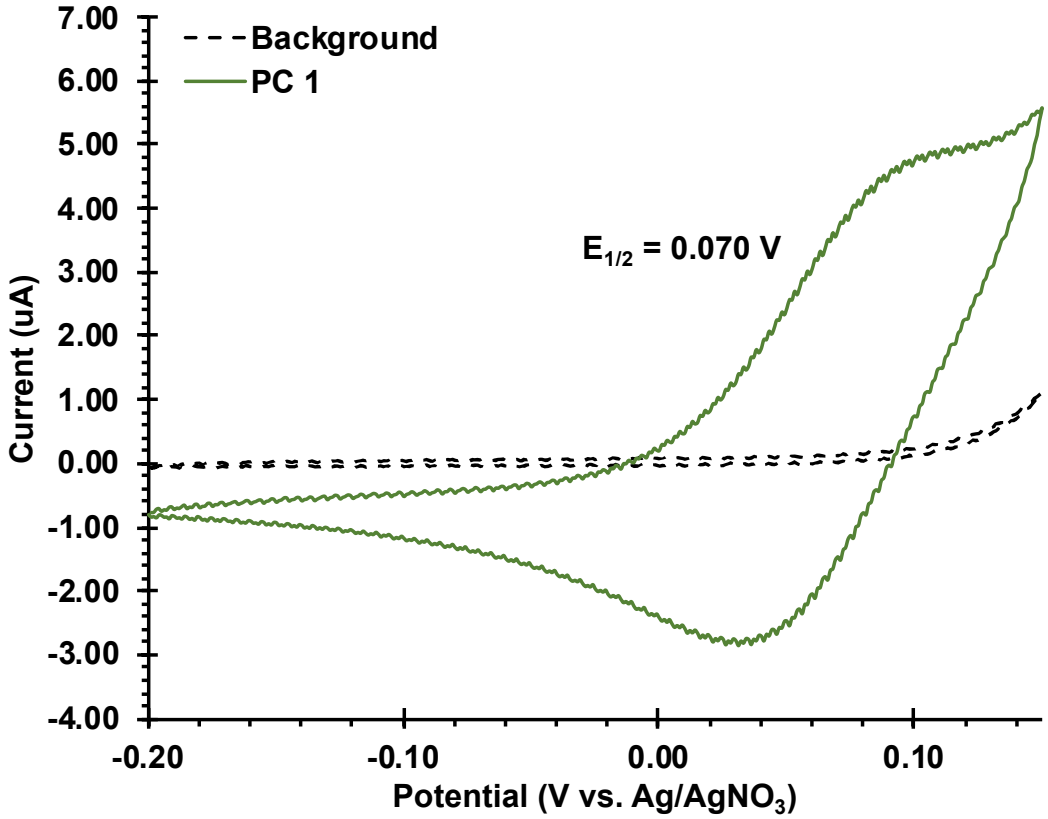

Figure S26. Cyclic voltammogram of PC **1** with supporting electrolyte = 0.094 M Bu_4NPF_6 and 0.006 M Bu_4NBr. Reference electrode = $Ag/AgNO_3$.

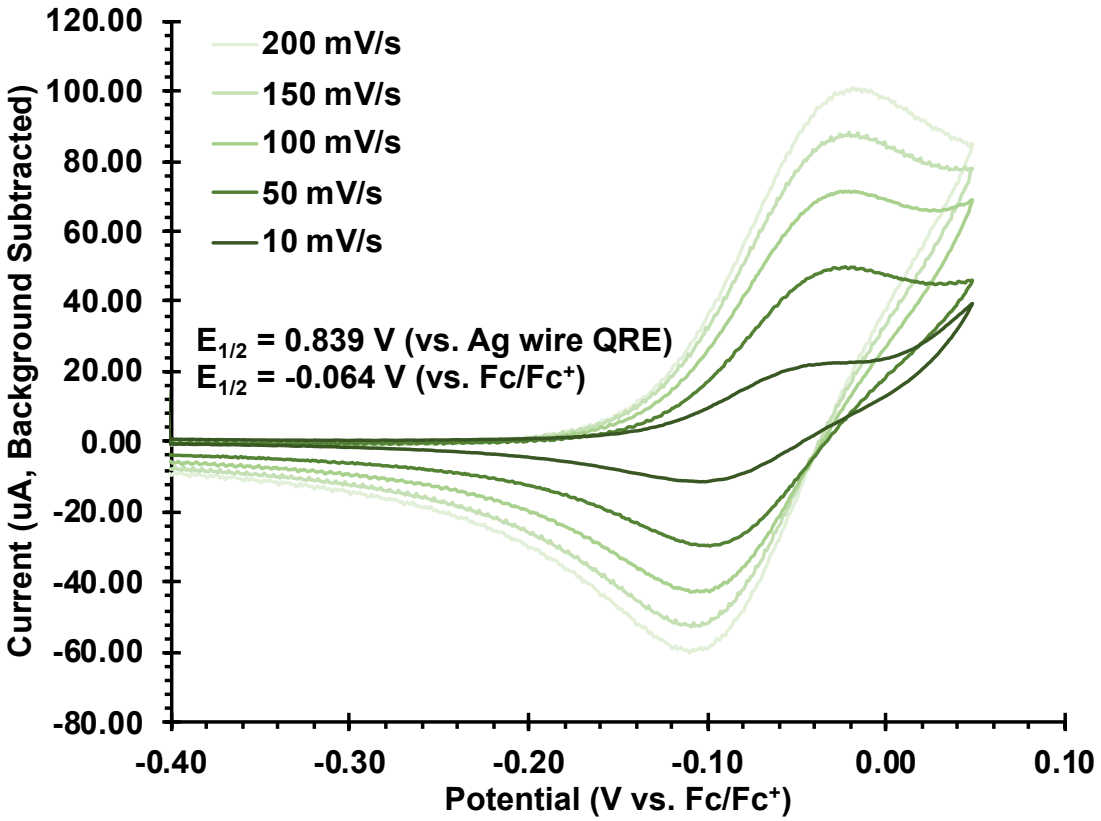

Figure S27. Cyclic voltammogram of PC **1** with supporting electrolyte = 0.094 M Bu_4NPF_6 and 0.006 M Bu_4NBr. Reference electrode = Ag wire quasi-reference electrode. Background subtraction to improve peak resolution was performed by measuring the background CV at each scan rate and subtracting it from each collected voltammogram of PC **1**.

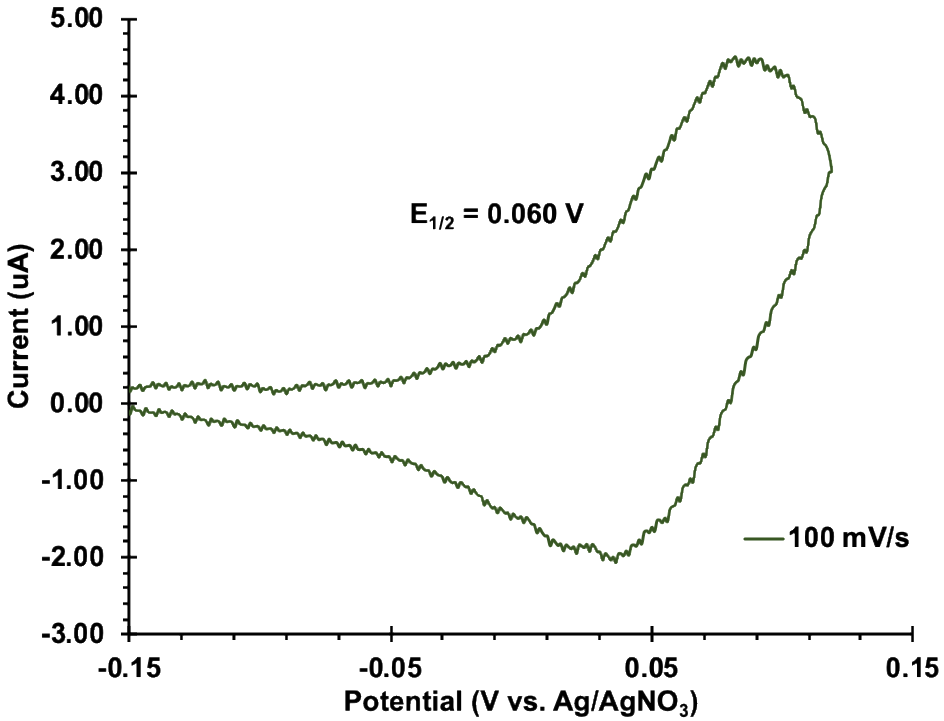

Figure S28. Cyclic voltammogram of PC **1** with supporting electrolyte = 0.094 M $LiPF_6$ and 0.006 M LiBr. Reference electrode = $Ag/AgNO_3$. Due to overlab of the $PC^{\bullet+}$/PC redox couple with the onset of bromide oxidation, background subtraction and curve smoothing were used to resolve the desired redox couple.

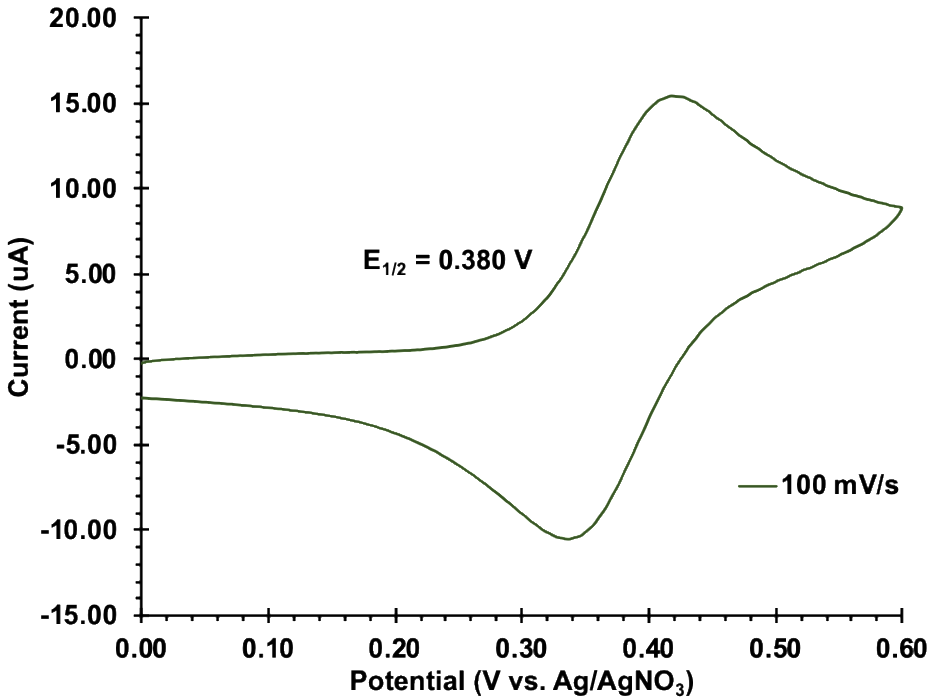

Figure S29. Cyclic voltammogram of PC **2** with supporting electrolyte = 0.1 M $LiPF_6$. Reference electrode = $Ag/AgNO_3$.

General Methods for Electrochemically Mediated O-ATRP (eO-ATRP)

eO-ATRP in U-Cells

The working electrode compartment of a U-cell – an electrochemical cell with two compartments separated by a fine or extra-fine glass frit – was charged with **1** (1.8 mg, 1.87 μmol, 0.1 eq) and a magnetic stir-bar. The cell was assembled with a working and reference electrode in the same compartment as **1**, and counter-electrode in the other compartment. After purging the cell for 15 minutes with N_2, a supporting electrolyte solution in DMAc (2 mL, 0.2 M, either 94% Bu_4NPF_6 and 6% Bu_4NBr, or $LiPF_6$) was added to both compartments of the cell, followed by addition of MMA (2 mL, 18.7 mmol, 1000 eq) to both compartments using standard Schlenk techniques to make the final concentration of supporting electrolyte 0.1 M. After addition of diethyl-2-bromo-2-methylmalonante (DBMM, 17.9 μL, 9.35 x 10^{-2} mmol, 5 eq), bulk electrolysis was performed overnight in the dark to generate the desired ratio of **1** to $\mathbf{1}^{\bullet+}$ prior to irradiation, and then irradiation was commenced.

eO-ATRP in 5-neck pear flasks

A 5-neck pear flask (Gamry Dr. Bob's cell) was charged with **1** (1.8 mg, 1.87 μmol, 0.1 eq) and a magnetic stir-bar. The cell was assembled with a glassy carbon working electrode, a platinum wire counter electrode – separated by a vycor frit – and a $Ag/AgNO_3$ reference electrode. After purging the cell for 15 minutes under a positive pressure of N_2, a solution in DMAc (2 mL), MMA (2 mL, 1000 eq, 18.7 mmol), DBMM (17.9 μL, 9.35 x 10^{-2} mmol, 5 eq), and $LiPF_6$ (60.8 mg, 0.1 M final concentration) was added to the cell using standard Schlenk techniques. Bulk electrolysis was performed overnight in the dark to generate the desired ratio of **1** to $\mathbf{1}^{\bullet+}$ prior to irradiation, and then irradiation was commenced.

General Method for Analysis of Kinetics and Molecular Weight Growth

To monitor polymerizations, 0.1 mL aliquots were removed periodically using a nitrogen purged syringe and needle. Aliquots were quenched in a deuterated chloroform containing 250 ppm butylated hydroxytoluene (BHT). These solutions were then transferred to an NMR tube for ^1H NMR analysis to determine the extent of monomer conversion. Afterwards, solutions were dried under compressed air and dissolved in unstabilized THF for GPC analysis to obtain number average molecular weight and dispersity.

Estimation of Excited State PC Concentration

The following calculations were performed to obtain a rough estimate of how much PC* forms upon irradiation of a solution of PC under conditions similar to those used in this work. First, to simplify the system, a solution without initiator or polymer was considered. In addition, the PC was considered to operate from a generic excited state (PC*), such that the singlet and triplet excited states – and the processes converting between them – did not have to be considered separately. Under these conditions, the concentration of PC* is impacted by (1) photoexcitation and (2) relaxation to the ground state.

Table S1. Reactions considered in the estimation of PC* concentrations.

Reaction	Scheme	Process
1	PC + hν ⟶ PC*	Photoexcitation
2	PC* ⟶ (k_relax) PC + hν	Relaxation

Assuming PC* reaches a steady state, the following equation can be written:

$$\frac{d[PC^*]}{dt} = I^o[PC] - k_{relax}[PC^*] = 0 \qquad \text{Eq. S1}$$

However, this equation can be further simplified considering that the reaction rate will likely be limited by either the concentration of catalyst or the photon flux into the reaction vessel. Data published for PC **1** suggests that this O-ATRP system lies in the flux limited regime, as changes in catalyst loading showed no impact on the observed rate of polymerization.[5] Further, in an investigation of the impact of light intensity in O-ATRP with PC **2**, it was shown that the observed rate of polymerization with this PC is dependent on light intensity.[1] Together, these data provide a strong indication that O-ATRP under these conditions is flux limited, allowing Equation S1 to be simplified.

$$\frac{d[PC^*]}{dt} = I^o - k_{relax}[PC^*] = 0 \qquad \text{Eq. S2}$$

Where I^o is the concentration of photons entering the reaction vessel in a given unit of time [mol $L^{-1}s^{-1}$). Solving Equation S2 for the concentration of PC*, one gets:

$$[PC^*] = \frac{I^o}{k_{relax}} \qquad \text{Eq. S3}$$

Here, k_{relax} can be related to the lifetime of the excited state. Since O-ATRP catalysts likely operate from the triplet excited state, this value can be written as:

$$k_{relax} = \frac{1}{\tau_t} \qquad \text{Eq. S4}$$

Thus, plugging Equation S4 into Equation S3, one gets:

$$[PC^*] = I^o \cdot \tau_t \qquad \text{Eq. S5}$$

Where τ_t is the triplet excited state lifetime. Since the triplet excited state lifetime for PC **1** has not been reported, those for two common O-ATRP PCs were considered instead (Figure S30). For PC **2**, τ_t = 480 μs, whereas τ_t = 4.3 μs for PC **3**.[7]

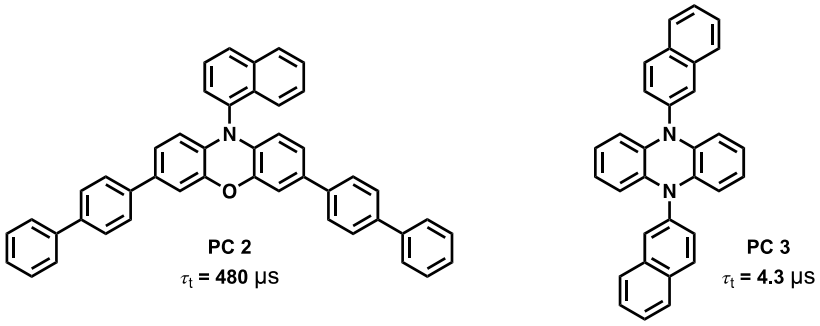

Figure S30. Structures and triplet excited state lifetimes of PCs used in the estimation of [PC*].

With these values known, we now need to know the photon flux for the LEDs used in this work. Since this value is challenging to obtain for a white light source and most of the light absorbed by the PC is under 500 nm, only the blue emission feature of the LEDs was considered for this calculation. Further, this blue feature was approximated by the emission of a similar blue LED (Figure S31), for which photon flux could be determined (14.5 μmol s^{-1}).[8] Since the blue portion of the white LED emission is about 2.5 times more intense than for the blue LED, the photon flux for this feature can be approximated as 36.3 μmol s^{-1}. Accounting for the reaction volume used in this work (4.0 mL), I^o is calculated from this value of photon flux to be 9.0 x 10^{-3} M s^{-1}.

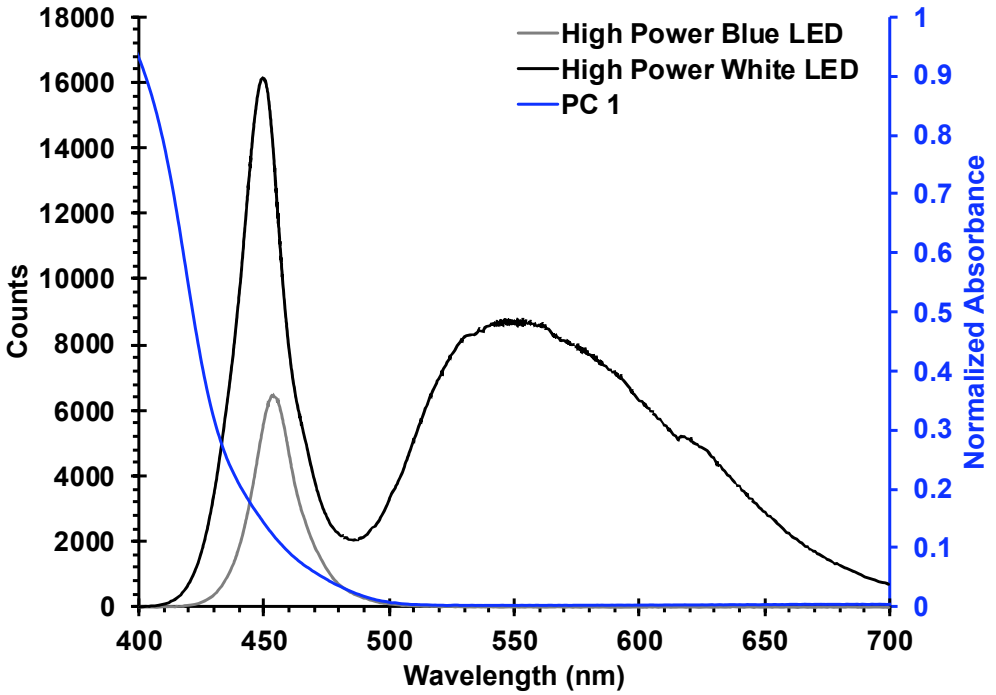

Figure S31. Qualitative emission spectra of the high-power white LEDs used in this work (black) and a similar model blue LED (grey). Overlay of the absorption spectrum of **1** in the polymerization solution (blue) shows the blue portion of the LED emission (peak around 450 nm) makes up the majority of the light absorbed by the PC. Solution composed of 0.04 mM **1** in 50/50 (*v/v*) DMAc/MMA with 0.094 M Bu_4NPF_6 and 0.006 M Bu_4NBr.

Finally, we can use these values of photon flux and triplet excited state lifetime to estimate the concentration of PC* under irradiation with a high-power white LED, which for **2** is about 4.3 x 10^{-6} M and for **3** is 4.0 x 10^{-8} M. Under the conditions used in this work (100 ppm PC), the concentration of PC is 4.6 x 10^{-4} M. Therefore, when PC **2** is used, about 0.9% of the total PC in solution is PC*, whereas when PC **3** is used, roughly 0.008% is in the form of PC*. Since the excited state lifetime of **1** is unknown and we therefore cannot know how much of **1** exists in solution as PC*, an electrochemical potential was chosen to generate 0.9% $PC^{\bullet+}$ ($E_{app} = E_{1/2} - 120$ mV) to ensure a sufficiently high concentration of $PC^{\bullet+}$ to effectively mediate deactivation.

Control Experiments

Hypothesis 1: Reduction of Tetra-n-butylammonium Cation

*Hypothesis: Photoexcited **1** reduces the tetrabutylammonium cation by single electron transfer to generate a reactive species that leads to undesirable side reactivity.*

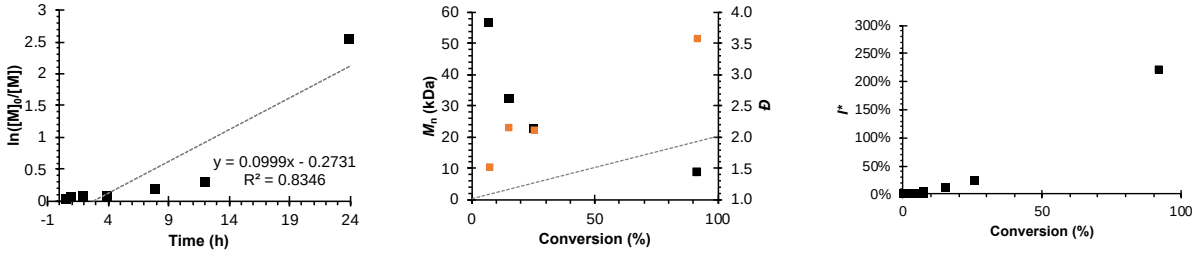

Figure S32. eO-ATRP performed in a U-cell with 0.094 M $LiPF_6$ and 0.006 M LiBr supporting electrolyte. Conditions: 2 mL DMAc, 2 mL MMA, 17.9 µL DBMM, 1.8 mg **1**. Working electrode = glassy carbon rod, counter electrode = Pt wire, reference electrode = 0.01 M $AgNO_3$/Ag in MeCN with 0.1 M Bu_4NPF_6, $E_{app} = E_{1/2} - 120$ mV (~1% $PC^{\bullet+}$). Polymerization irradiated with a high-power white LED. Key: First order kinetics plot (left), molecular weight (black) and dispersity (orange) as a function of monomer conversion (center), and initiator efficiency as a function of monomer conversion (right).

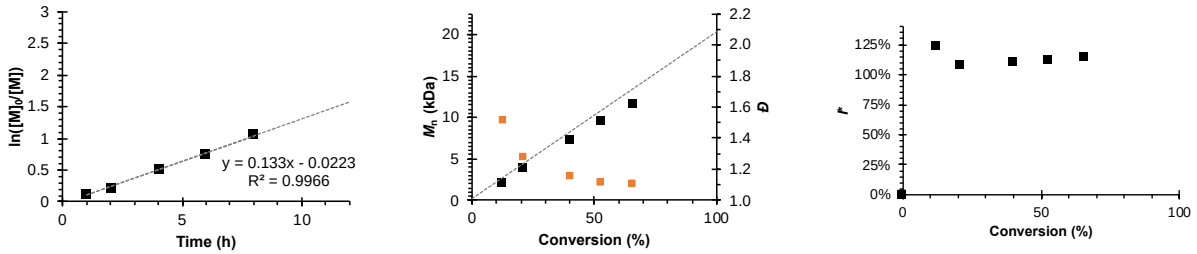

Figure S33. O-ATRP performed in a 20 mL scintillation vial with 0.094 M $LiPF_6$ and 0.006 M LiBr supporting electrolyte. Conditions: 2 mL DMAc, 2 mL MMA, 17.9 µL DBMM, 1.8 mg **1**. Polymerization irradiated in a white LED beaker. Key: First order kinetics plot (left), molecular weight (black) and dispersity (orange) as a function of monomer conversion (center), and initiator efficiency as a function of monomer conversion (right).

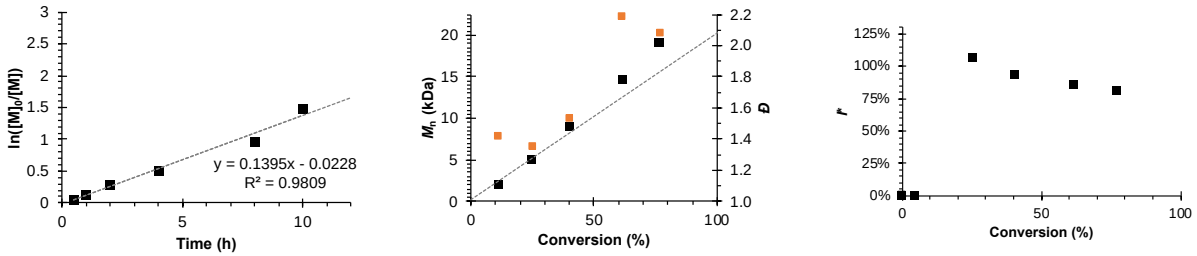

Figure S34. eO-ATRP performed in a U-cell with 0.1 M $LiPF_6$ supporting electrolyte. Conditions: 2 mL DMAc, 2 mL MMA, 17.9 µL DBMM, 1.8 mg **1**. Working electrode = glassy carbon rod, counter electrode = Pt wire, reference electrode = 0.01 M $AgNO_3$/Ag in MeCN with 0.1 M Bu_4NPF_6, $E_{app} = E_{1/2} - 120$ mV (~1% $PC^{\bullet+}$). Polymerization irradiated with a high-power white LED. Key: First order kinetics plot (left), molecular weight (black) and dispersity (orange) as a function of monomer conversion (center), and initiator efficiency as a function of monomer conversion (right).

Hypothesis 2: Oxidation of MMA at the Working Electrode

Hypothesis: MMA is oxidized at the working electrode to produce a reactive species that initiates undesired side reactions, leading to poor polymerization control.

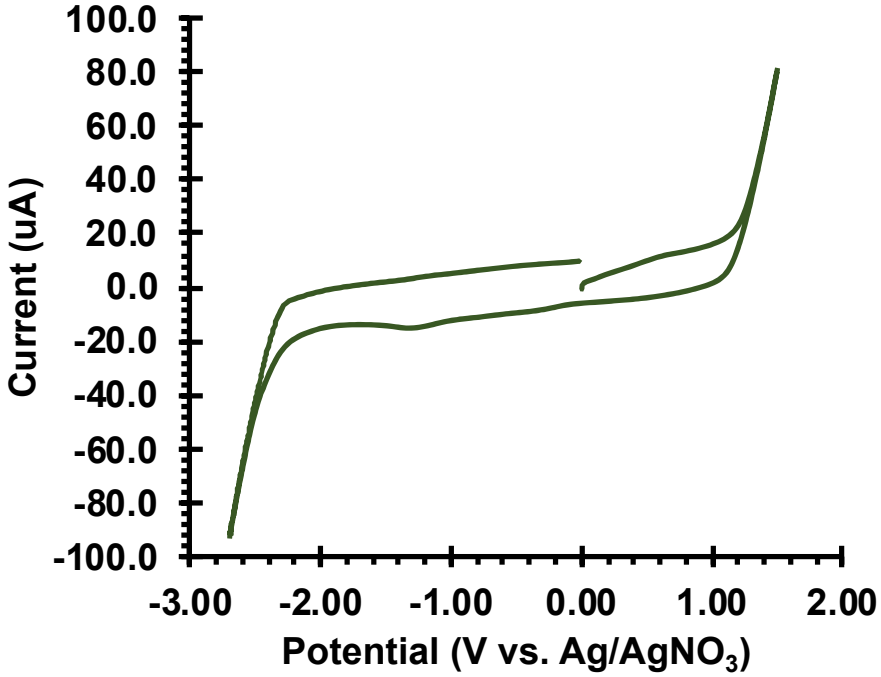

Figure S35. Cyclic voltammogram of 50/50 (*v/v*) DMAc and MMA with 0.1 M Bu_4NPF_6 at a glassy carbon working electrode.

Hypothesis 3: Oxidation of DBMM at the Working Electrode

Hypothesis: DBMM is oxidized at the working electrode to produce a reactive species that initiates undesired side reactions, leading to poor polymerization control.

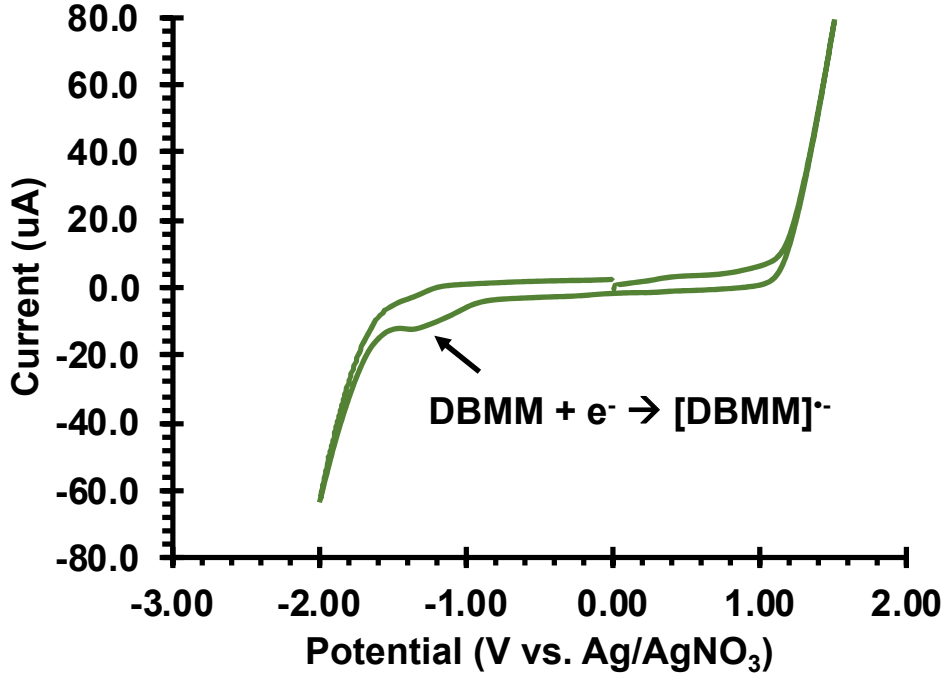

Figure S36. Cyclic voltammogram of 13 mM DBMM in 50/50 (*v/v*) DMAc and MMA with 0.1 M Bu_4NPF_6 at a glassy carbon working electrode.

Hypothesis 4: Bromide Oxidation at the Working Electrode

Hypothesis: Bromide is oxidized at the working electrode to produce a reactive species that initiates undesired side reactions, leading to poor polymerization control.

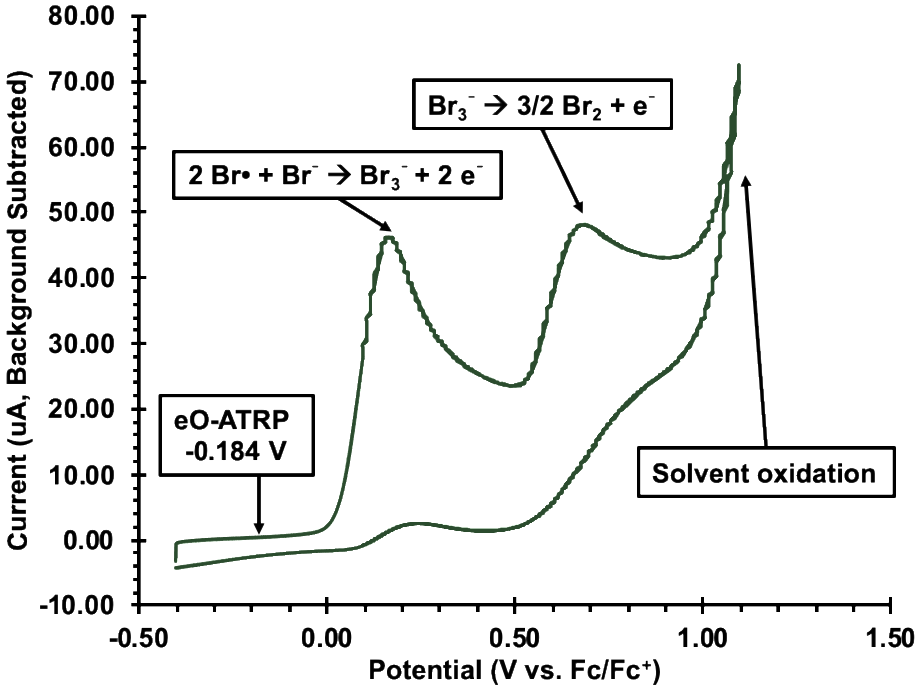

Figure S37. Cyclic voltammogram bromide ion in 50/50 (*v/v*) DMAc and MMA with 0.1 M Bu_4NPF_6 (94%) and Bu_4NBr (6%) at a glassy carbon working electrode. Since the refence electrode used was a silver wire QRE, potentials are reported vs. the ferrocene/ferrocenium couple (Fc/Fc^+). For reference, eO-ATRP under these conditions is performed at -0.184 V, corresponding to $E_{1/2}(\mathbf{1}^{\bullet+}/\mathbf{1})$ – 120 mV.

In addition to the electrochemical control shown above, a control reaction was performed to test whether bromide oxidation might cause an undesired polymerization at the relevant electrochemical potential for eO-ATRP. For this experiment, a typical polymerization solution was prepared in a U-cell with DMAc (2 mL), MMA (2 mL, 1000 eq, 18.7 mmol), DBMM (17.9 µL, 9.35×10^{-2} mmol, 5 eq), and supporting electrolyte (0.1 M Bu_4NPF_6 (94%) and Bu_4NBr (6%)). To prevent any undesired reactivity due to stray light entering the flask, no **1** was added to this solution. The cell was then kept in the dark and electrolysis ($E_{app} = E_{1/2}(\mathbf{1}^{\bullet+}/\mathbf{1})$ – 120 mV) commenced. After 24h, an aliquot of the reaction mixture was removed for ^{1}H NMR analysis. No monomer conversion was observed.

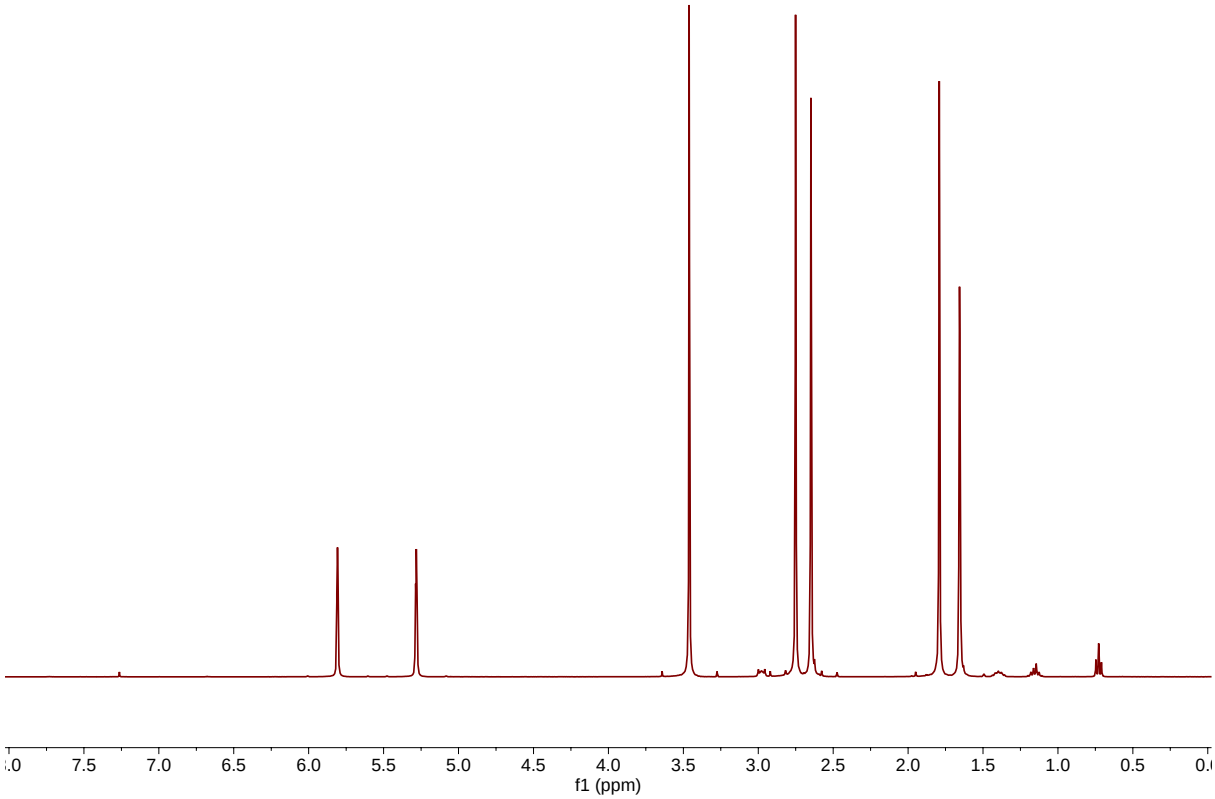

Figure S38. ^{1}H NMR of the control polymerization testing for the impact of bromide oxidation at 24 h of electrolysis.

Hypotheses 5 – 7: Photoexcitation of the Radical Cation

*Hypothesis: The radical cation of **1** is photoexcited to generate a strongly oxidizing state, which causes side reactivity by oxidizing either DMAc (hypothesis 5), the radical chain end (hypothesis 6), or bromide ion (hypothesis 7).*.

- Currently, no evidence exists to disprove the oxidation of DMAc or the radical chain end, though a kinetic argument can be used to eliminate oxidation of the chain end as a viable hypothesis (see main text).
- To test whether the oxidation of bromide could be problematic, the following experiment was devised (note that this experiment is not intended to shed light on what would cause the bromide oxidation; it is simply meant to test whether the resulting bromine radical would initiate a polymer chain under relevant conditions):

For this experiment, a typical polymerization solution was prepared in a U-cell with DMAc (2 mL), MMA (2 mL, 1000 eq, 18.7 mmol), and supporting electrolyte (0.1 M Bu_4NPF_6 (94%) and Bu_4NBr (6%)). To prevent any undesired reactivity due to stray light entering the flask, no **1** was added to this solution. The cell was then kept in the dark and electrolysis (E_{app} = 1 V vs Ag wire QRE, ~ 0.1 V vs Fc/Fc^+) commenced. After 48h, an aliquot of the reaction mixture was removed for ^{1}H NMR analysis and the cell inspected. A white film was observed on the surface of the

working electrode, and NMR analysis showed about 2% monomer conversion. Both samples were dried, dissolved in THF, and analyzed by GPC; the results are below.

Table S2. Results from the control polymerization of MMA by electrolysis of bromide to make bromine radical.

Sample	Time	Conv. (%)	M_n (kDa)	$Đ$
Aliquot[a]	48 h	2	24.4	1.23
			47.7	1.39
Film	48 h	N/A	53.9	1.99

[a]GPC results for this sample were multimodal, so analysis of all relevant peaks is reported.

Hypothesis 8: Competitive Ion-Pairing

Hypothesis: Competitive ion pairing between Br^- and PF_6^- hinders formation of the proposed deactivating species $PC^{\bullet+}Br^-$. As a result, the rate of deactivation decreases, resulting in poor polymerization control.

To investigate the impact of the $LiPF_6$ supporting electrolyte on O-ATRP, a polymerization was carried out in the following manner. A 20 mL scintillation vial was charged with **1** (1.8 mg, 1.87 µmol, 0.1 eq) and a magnetic stir-bar. In a nitrogen filled glovebox, $LiPF_6$ (60.8 mg, 0.4 mmol, 0.1 M final concentration) was weighed into the vial, followed by the addition of DMAc (2 mL), MMA (2 mL, 18.7 mmol, 1000 eq), and DBMM (17.9 µL, 9.35 x 10^{-2} mmol, 5 eq). The reaction was then irradiated using a white LED beaker and aliquots removed periodically to monitor the progression of the polymerization.

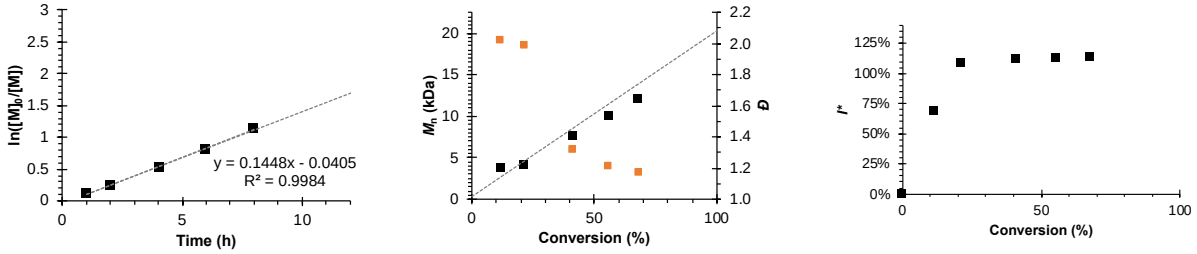

Figure S39. Results of the O-ATRP of MMA in the presence of 0.1 M $LIPF_6$. Key: First order kinetics plot (left), molecular weight (black) and dispersity (orange) as a function of monomer conversion (center), and initiator efficiency as a function of monomer conversion (right).

Hypothesis 9: Insufficient Separation of the Counter Electrode

Hypothesis: The glass frit separator in the U-cell is an insufficient barrier to prevent diffusion of reaction components towards the counter electrode on the timescale of a polymerization (~24h – 48h). As a result, key components, such as the PC or $PC^{\bullet+}$, undergo degradation at the counter electrode, resulting in poor control over the polymerization.

For reaction setup, see previous section - General Methods for Electrochemically Mediated O-ATRP (eO ATRP). In this experiment, a $Ag/AgNO_3$ reference electrode was used, and $E_{app} = E_{1/2}$ – 120 mV. Irradiation was carried out using an 80x40 light beaker with 9 LED segments.

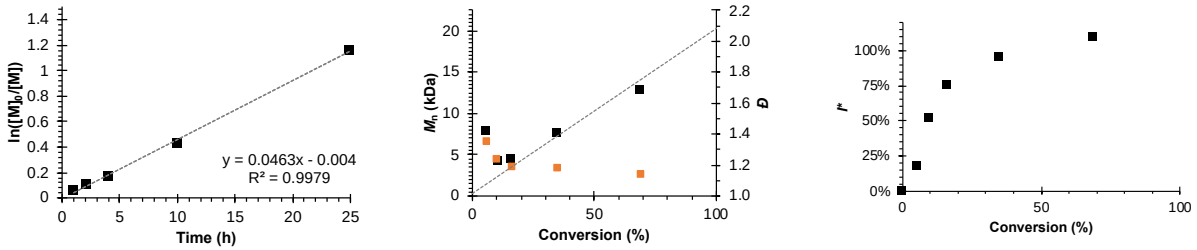

Figure S40. Results of eO-ATRP of MMA using a new apparatus featuring separation of the counter electrode using a vycor glass frit. Key: First order kinetics plot (left), molecular weight (black) and dispersity (orange) as a function of monomer conversion (center), and initiator efficiency as a function of monomer conversion (right).

Control Polymerizations

The following polymerizations were performed systematically eliminating one reaction component from eO-ATRP at a time to test the effect of each component on the overall reaction. For reaction setup, see previous section - General Methods for Electrochemically Mediated O-ATRP (eO ATRP). In each experiment below, a $Ag/AgNO_3$ reference electrode was used, and $E_{app} = E_{1/2} – 120$ mV. Irradiation was carried out using a white LED well (80 mm x 40 mm) with 9 LED segments.

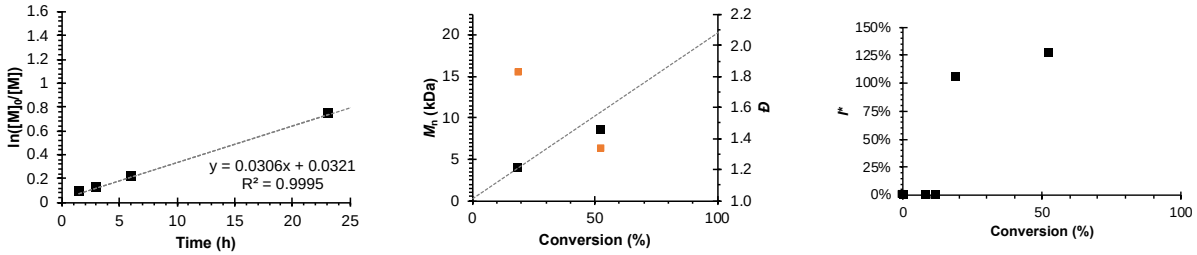

Figure S41. Results of O-ATRP in the presence of 0.1 M $LiPF_6$ without electrolysis. Key: First order kinetics plot (left), molecular weight (black) and dispersity (orange) as a function of monomer conversion (center), and initiator efficiency as a function of monomer conversion (right).

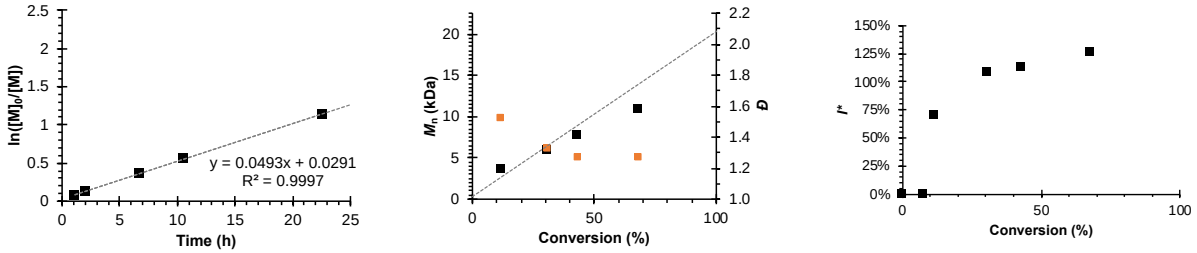

Figure S42. Results of O-ATRP in a 5-neck pear flask without supporting electrolyte or electrolysis. Key: First order kinetics plot (left), molecular weight (black) and dispersity (orange) as a function of monomer conversion (center), and initiator efficiency as a function of monomer conversion (right).

In addition to the experiments above, control reactions eliminating the PC, DBMM, light, and PC and light were carried out. The results of these experiments are provided in the main text.

Supplemental Polymerization Data

eO-ATRP Lighting Screen

For reaction setup, see previous section - General Methods for Electrochemically Mediated O-ATRP (eO ATRP). In each experiment below, a $Ag/AgNO_3$ reference electrode was used, and $E_{app} = E_{1/2} – 120$ mV. Irradiation was carried out using the setup described in the respective figure caption.

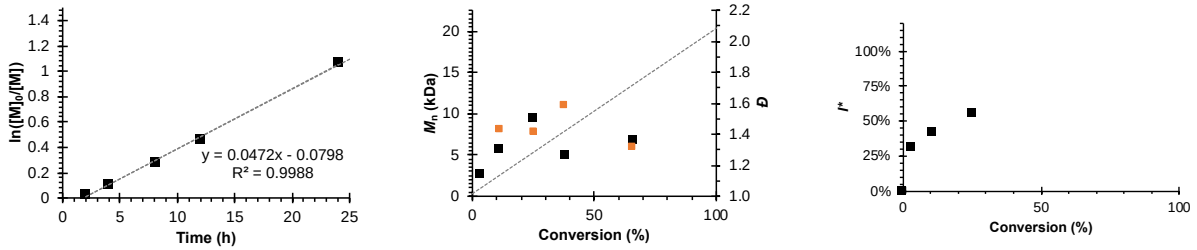

Figure S43. Polymerization results from eO-ATRP of MMA using a 80x40 light well (9 LED segments) at 50% irradiation intensity, which was achieved by use of an in-line LED dimmer.[1] Key: First order kinetics plot (left), molecular weight (black) and dispersity (orange) as a function of monomer conversion (center), and initiator efficiency as a function of monomer conversion (right).

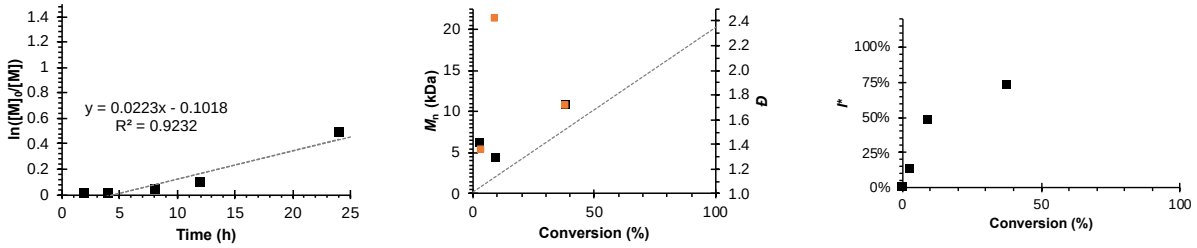

Figure S44. Polymerization results from eO-ATRP of MMA using a 80x40 light well (9 LED segments) at 5% irradiation intensity, which was achieved by use of an in-line LED dimmer.[1] Key: First order kinetics plot (left), molecular weight (black) and dispersity (orange) as a function of monomer conversion (center), and initiator efficiency as a function of monomer conversion (right).

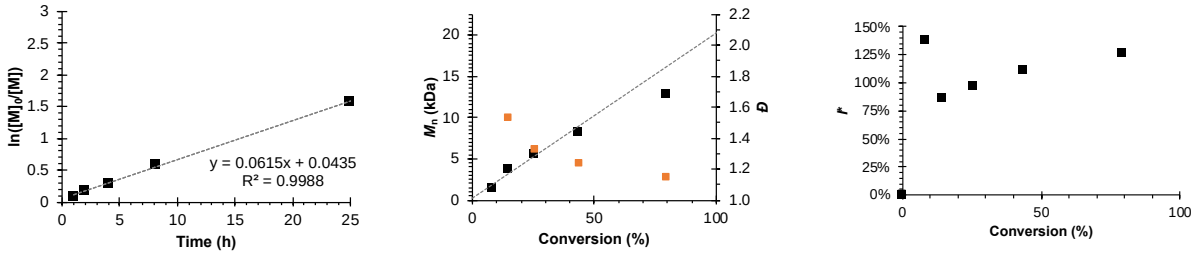

Figure S45. Polymerization results from eO-ATRP of MMA using a 80x40 light well with a larger concentration of LEDs than used previously (15 LED segments) to test the impact of increased irradiation intensity. Key: First order kinetics plot (left), molecular weight (black) and dispersity

(orange) as a function of monomer conversion (center), and initiator efficiency as a function of monomer conversion (right).

Data from the three figures above is replotted below for more facile comparison of the data.

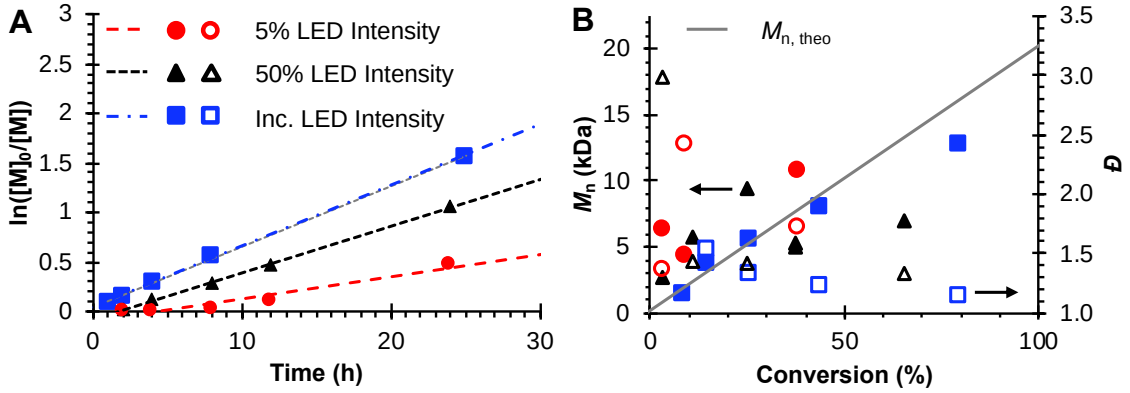

Figure S46. Comparison of kinetics (A) as well as molecular weight (filled markers) and *Đ* (hollow markers) evolution (B) for eO-ATRP under irradiation of varying intensity (blue squares: increased intensity, black triangles: 50% intensity, red circles: 5% intensity). Conditions: [MMA]:[DBMM]:[**1**] = 1000:5:0.1, 2 mL MMA, 2 mL DMAc, supporting electrolyte = 0.1 M $LiPF_6$. Reactions performed in a 5-neck pear flask with working electrode = glassy carbon, counter electrode = Pt wire, reference electrode = $Ag/AgNO_3$, and $E_{app} = E_{1/2} - 120$ mV. See supporting information for irradiation conditions (section: eO-ATRP lighting screen).

Table S3. Results for eO-ATRP[a] performed under various light intensities. Entry 4 from Table C provided for comparison to eO-ATRP under normal irradiation conditions.

Entry	LED Intensity[b]	Time (h)	Conv. (%)	$M_{n,\,theo}$ (kDa)	$M_{n,\,GPC}$ (kDa)	$Đ^c$	I^* (%)[d]
4	unchanged	25	69	14.0	12.8	1.17	110
S1	increased[e]	25	79	16.1	12.8	1.14	126
S2	50%[f]	24	66	13.4	6.88	1.32	194
S3	5%[f]	24	38	7.84	10.8	1.72	73

[a]General conditions unless otherwise stated: [MMA]:[DBMM]:[**1**] = 1000:5:0.1, 2 mL MMA, 2 mL DMAc, SE = 0.1 M $LiPF_6$. Reactions performed in a 5-neck pear flask with working electrode = glassy carbon, counter electrode = Pt wire, reference electrode = $Ag/AgNO_3$, and $E_{app} = E_{1/2} - 120$ mV. [b]LED intensity relative to an 80mm x 40mm white LED well with 9 LED segments. [c]Calculated by M_w / M_n. [d]Calculated by $M_{n,\,theo} / M_{n,\,GPC}$. [e]Increased LED intensity achieved by lining an 80mm x 40mm white LED well with 15 LED segments. [f]Decreased LED intensity achieved by used of an in-line dimmer with an 80mm x 40mm white LED well (9 LED segments, see *Experimental Equipment* in SI).

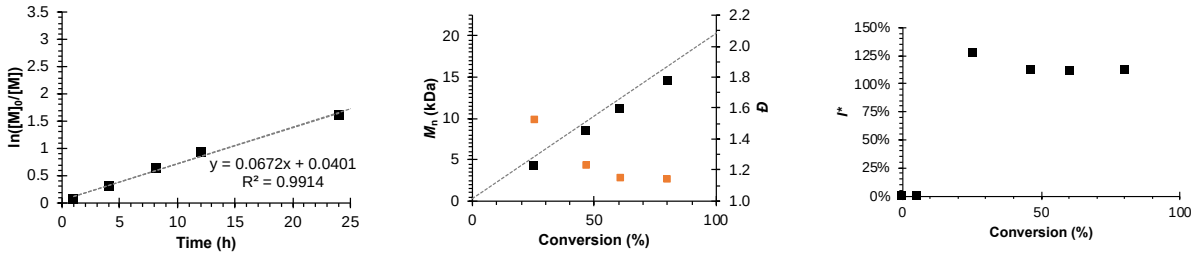

Figure S47. Polymerization results from eO-ATRP of MMA using a 70x50 light well with the same number of LED segments (9 LED segments) to test the impact of having the LEDs closer to the reaction. Key: First order kinetics plot (left), molecular weight (black) and dispersity (orange) as a function of monomer conversion (center), and initiator efficiency as a function of monomer conversion (right).

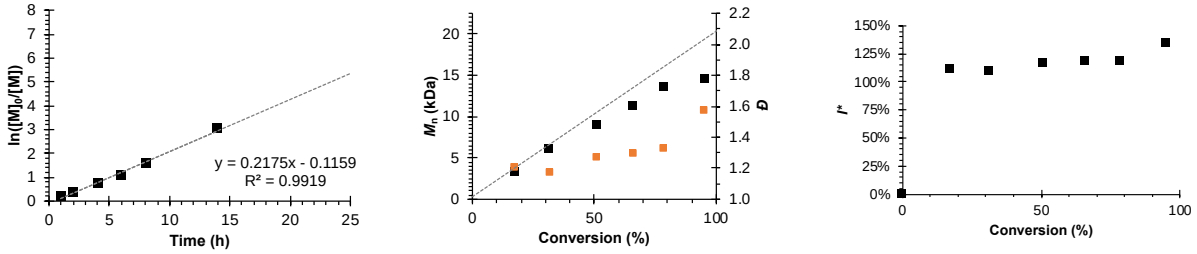

Figure S48. Polymerization results from eO-ATRP of MMA using a high-power white LED reactor (see Experimental Equipment section) to test the impact of further increased irradiation intensity. Key: First order kinetics plot (left), molecular weight (black) and dispersity (orange) as a function of monomer conversion (center), and initiator efficiency as a function of monomer conversion (right).

To investigate the impact of this new irradiation apparatus on O-ATRP in the absence of electrolysis, a control polymerization was carried out under the same conditions – in a 5-neck flask, using the same light reactor – but in the absence of the electrodes and applied electrochemical potential. To account for any effects that could be attributed to the supporting electrolyte, $LIPF_6$ (0.1 M) was added to this polymerization.

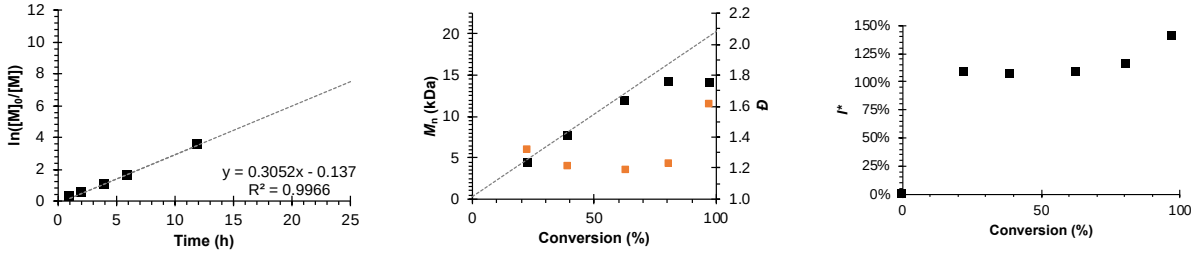

Figure S49. Polymerization result from a control reaction (O-ATRP with 0.1 M $LIPF_6$) in the high-power LED reactor. Key: First order kinetics plot (left), molecular weight (black) and dispersity (orange) as a function of monomer conversion (center), and initiator efficiency as a function of monomer conversion (right).

eO-ATRP At a More Oxidizing Potential

To investigate whether increasing the concentration of $PC^{\bullet+}$ improves polymerization control, eO-ATRP was performed at a more oxidizing potential: $E_{app} = E_{1/2} - 60$ mV, corresponding to ~10% radical cation relative to the total concertation of **1**. Irradiation was carried out using the high-power white LED apparatus.

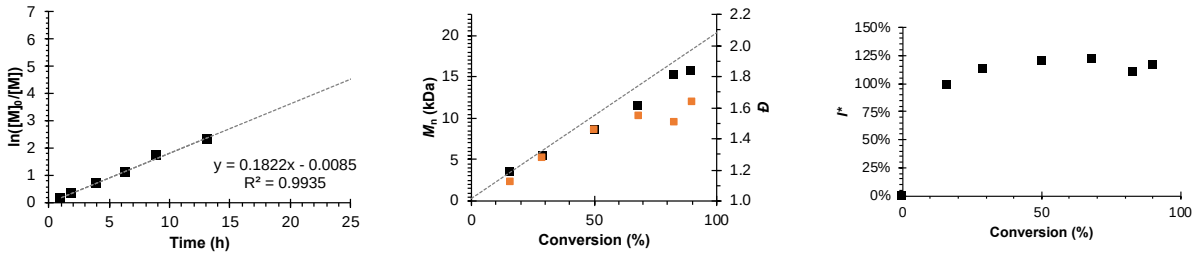

Figure S50. Polymerization results for eO-ATRP of MMA carried out at a more oxidizing potential to further increase [$PC^{\bullet+}$]. Key: First order kinetics plot (left), molecular weight (black) and dispersity (orange) as a function of monomer conversion (center), and initiator efficiency as a function of monomer conversion (right).

For facile comparison, the data in Figure S50 is replotted below with data for polymerizations under the same conditions but at a less oxidizing E_{app} and without electrolysis.

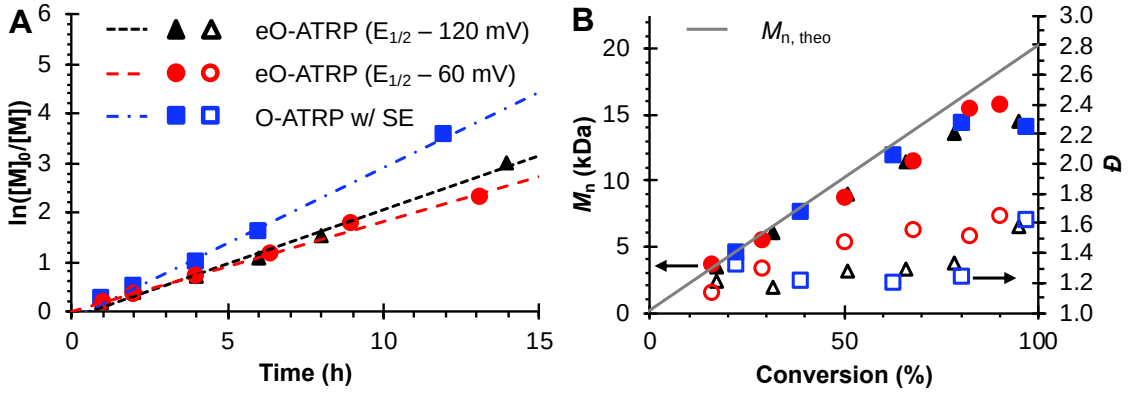

Figure S51. Plot of the natural logarithm of monomer (M) consumption over time (A). Molecular weight (filled markers) and *Đ* (hollow markers) evolution (B) for eO-ATRP at two applied potentials (black triangles: $E_{app} = E_{1/2} - 120$ mV, red circles: $E_{app} = E_{1/2} - 60$ mV) and O-ATRP with supporting electrolyte (blue squares), all in a high-power light reactor. Conditions: [MMA]:[DBMM]:[**1**] = 1000:5:0.1, 2 mL MMA, 2 mL DMAc, SE = 0.1 M $LiPF_6$. Reactions performed in a 5-neck pear flask and irradiated with a high-power white LED (see *Experimental Equipment* in SI). For eO-ATRP, working electrode = glassy carbon, counter electrode = Pt wire, and reference electrode = $Ag/AgNO_3$.

Polymerizations with PC **2**

To understand if observations related to eO-ATRP are applicable to other PC families, eO-ATRP was performed with PC **2**. For general reaction setup, see previous section - General Methods for Electrochemically Mediated O-ATRP (eO ATRP). For eO-ATRP, a 5-neck pear flask apparatus

was employed with a $Ag/AgNO_3$ reference electrode, and $E_{app} = E_{1/2} - 60$ mV. For O-ATRP in the presence of supporting electrolyte, a 5-neck pear flask was used without electrodes or an applied potential. Irradiation in both cases was carried out using an 80 mm x 40 mm white LED well with 9 LED segments. [MMA]:[DBMM]:[**2**] = 1000:5:1.

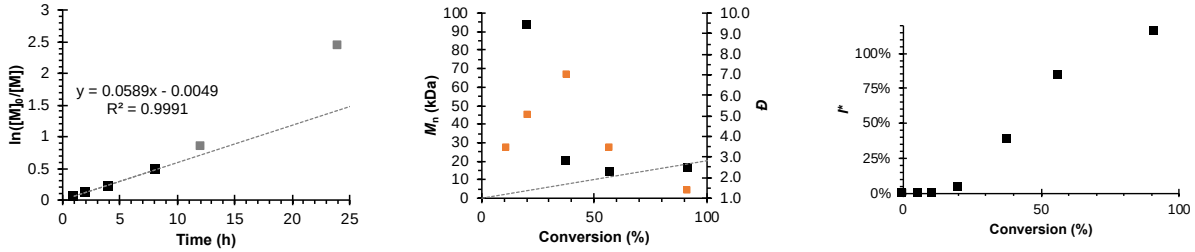

Figure S52. Polymerization results from eO-ATRP of MMA using PC **6** with $E_{app} = E_{1/2} - 60$ mV. Key: First order kinetics plot (left), molecular weight (black) and dispersity (orange) as a function of monomer conversion (center), and initiator efficiency as a function of monomer conversion (right).

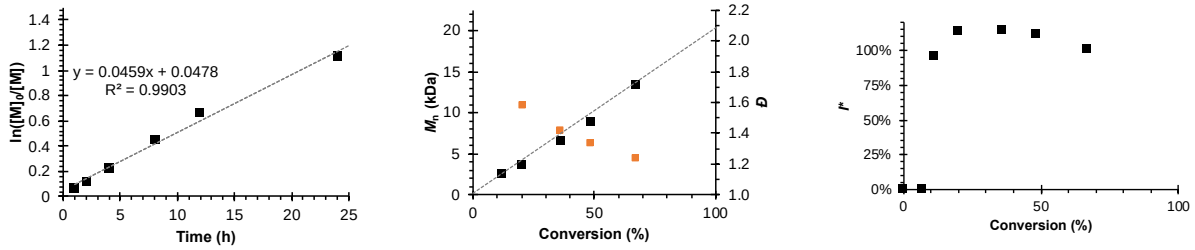

Figure S53. Polymerization results from O-ATRP of MMA using PC **2** in the presence of 0.1 M $LiPF_6$. Key: First order kinetics plot (left), molecular weight (black) and dispersity (orange) as a function of monomer conversion (center), and initiator efficiency as a function of monomer conversion (right).

eO-ATRP with a Chloride Supporting Electrolyte

To investigate the compatibility of eO-ATRP with a chloride supporting electrolyte, eO-ATRP was performed in the presence of 0.1 M tetra-n-butylammonium chloride (Bu_4NCl). For reaction setup, see previous section - General Methods for Electrochemically Mediated O-ATRP (eO ATRP). In this experiment, a 5-neck pear flask apparatus was employed, a $Ag/AgNO_3$ reference electrode was used, and $E_{app} = E_{1/2} - 120$ mV. Irradiation was carried out using an 80 mm x 40 mm white LED well with 9 LED segments.

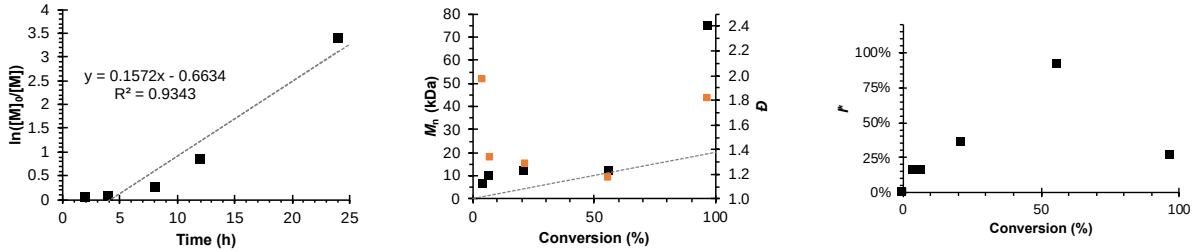

Figure S54. Polymerization results from eO-ATRP of MMA where the supporting electrolyte is 0.1 M Bu_4NCl. Key: First order kinetics plot (left), molecular weight (black) and dispersity (orange) as a function of monomer conversion (center), and initiator efficiency as a function of monomer conversion (right).

References

[1] M. D. Ryan, R. M. Pearson, T. A. French and G. M. Miyake, *Macromolecules*, 2017, **50**, 4616-4622.

[2] M. Kudisch, C.-H. Lim, P. Thordarson, G.M. Miyake, *J. Am. Chem. Soc.* **2019**, *141*, 19479.

[3] J. C. Theriot, C. H. Lim, H. Yang, M. D. Ryan, C. B. Musgrave and G. M. Miyake, *Science*, 2016, **352**, 1082-1086.

[4] B. G. McCarthy, R. M. Pearson, C. H. Lim, S. M. Sartor, N. H. Damrauer and G. M. Miyake, *J. Am. Chem. Soc.*, 2018, **140**, 5088-5101.

[5] J. P. Cole, C. R. Federico, C. H. Lim and G. M. Miyake, *Macromolecules*, 2019, **52**, 747-754.

[6] R. M. Pearson, C. H. Lim, B. G. McCarthy, C. B. Musgrave and G. M. Miyake, *J. Am. Chem. Soc.*, 2016, **138**, 11399-11407.

[7] Y. Du, R. M. Pearson, C. H. Lim, S. M. Sartor, M. D. Ryan, H. S. Yang, N. H. Damrauer and G. M. Miyake, *Chem. Eur. J.*, 2017, **23**, 10962.

[8] Specifications Sheet for LZ4-00B208 457 nm LED, https://www.osram.us/ledengin/products/luxigen/lz4.jsp, (Accessed April 2020).